Accepted Manuscript

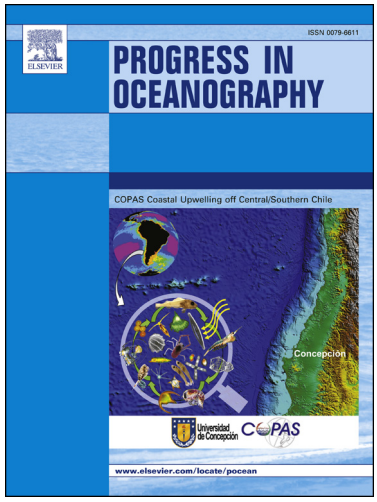

Aspects of the Antarctic Circumpolar Current dynamics investigated with drifter data

M. Trani, P. Falco, E. Zambianchi, J.B. Sallée

PII: S0079-6611(14)00086-X
DOI: http://dx.doi.org/10.1016/j.pocean.2014.05.001
Reference: PROOCE 1427

To appear in: *Progress in Oceanography*

Received Date: 20 August 2013
Revised Date: 7 April 2014
Accepted Date: 4 May 2014

Please cite this article as: Trani, M., Falco, P., Zambianchi, E., Sallée, J.B., Aspects of the Antarctic Circumpolar Current dynamics investigated with drifter data, *Progress in Oceanography* (2014), doi: http://dx.doi.org/10.1016/j.pocean.2014.05.001

Aspects of the Antarctic Circumpolar Current dynamics investigated with drifter data

M. Trani[1], P. Falco[1], E. Zambianchi[1], and J.B. Sallée[2,3]

[1] Department of Science and Technology, University of Naples "Parthenope," Centro Direzionale, Isola C4, IT-80143 Naples, Italy
[2] Sorbonne Universités (Paris 6, UPMC)-CNRS-IRD-MNHN, Lab. LOCEAN-IPSL, 4 place Jussieu, 75252 Paris Cedex 05 France
[3] British Antarctic Survey, High Cross, Madingley Road, CB30ET, Cambridge, UK

Corresponding author address: Marilisa Trani,
Department of Science and Technology, University of Naples "Parthenope," Centro Direzionale, Isola C4, IT-80143 Naples, Italy. E-mail: marilisa.trani@uniparthenope.it

Keywords: Southern Ocean; drifters; eddy flux; subduction; topographic effects.

Abstract

Interactions between eddies and mean flow are essential to close the momentum budget of the Southern Ocean, as well as to determine the structure of the global meridional overturning circulation. Both the structure of the Antarctic Circumpolar Current and the eddy dynamics arising at its heart are importantfor water-mass circulation and global ocean ventilation, and therefore for the global climate. However, the characterization of the eddy fields of heat and momentum are still poorly sampled by direct observations, and are difficult to accurately resolve or parameterize in numerical models. Here we present observation-based eddy statistics and eddy heat flux (EHF) from a consistent dataset, and estimate Southern Ocean surface EHF from direct measurements without any parameterization assumption. Observations obtained from near-surface drifters represent a very useful dataset to analyze the eddy field because of their ability to catch a large number of scales of motion while providing a quasi-synoptic coverage of the investigated area. Differences between winter and summer distributions of mean velocities, mean kinetic energy and eddy kinetic energy are shown to be strongly constrained by bottom topography and suggest a winter shift of the polar front in specific areas around the circumpolar belt. Overall, the flow follows the contours of constant planetary vorticity set by the depth of the ocean, and creates anisotropy in eddy dispersion with maximum dispersion along these contours. Furthermore, eddy–mean flow interactions are strongly influenced by topography, with eddies having a tendency to accelerate jets upstream of ridges, and decelerate them further downstream. These strong regional variabilities introduced by topography affect the flux of heat induced by eddies, and therefore affect formation and subduction of the main surface and intermediate Southern Ocean water masses. Integrated over the Southern Ocean, subduction of water masses induced by EHF appears as an order on component for the Southern Ocean thermocline ventilation. Our results based on direct

observations emphasizes, once more, the importance of continuing sustained effort to better represent the effect of mesoscale eddies in a coarse climate model, if we are to represent and predict future climate.

1. Introduction

The Southern Ocean plays a central role in the ventilation of deep and intermediate layers of the world's oceans. This role is closely linked to the presence of the Antarctic Circumpolar Current (ACC), which connects the major ocean basins and contributes to the existence of the global overturning circulation (Sloyan and Rintoul, 2001a; Lumpkin and Speer, 2007). The upward tilting of density surfaces associated with the geostrophic flow of the ACC creates a route for dense water to reach the ocean surface layer at high latitudes. While these dense waters are uplifted to the surface, they are transformed into denser or lighter water by the combined effect of air–sea fluxes, wind-driven Ekman fluxes, and eddy fluxes, before being subducted again to ventilate the ocean interior (Karsten and Marshall, 2002a; Bryden and Cunningham, 2003; Marshall and Radko, 2003; Sallée et al., 2010).

Mesoscale eddies strongly control the ACC circulation, with eddy-induced transports of heat and momentum actively participating in both the dynamic and thermodynamic balances of the ACC system (Munk and Palmen, 1951; Johnson and Bryden, 1989; Marshall et al., 1993). Despite its importance, the structure of the Southern Ocean eddy field is complex and not well understood, and thought to be locally shaped by mean flow and bottom topography (Ivchenko et al., 1996; Stammer, 1998; Hughes and Ash, 2001; Olbers et al., 2004; Sallée et al., 2011). Great efforts have been undertaken to better understand the nature of the relations between eddy kinetic energy (EKE), mean flow, and bottom topography, and in particular their influence on the mixing of properties across the ACC; however, the processes at play are still unclear (Shuckburgh et al., 2009; Lu and Speer, 2010; Naveira-Garabato et al., 2011; Sallée et al., 2011).

Satellite maps of sea surface temperature (SST) and sea surface height (SSH) first revealed the complexity and transient nature of ACC jets, strongly dominated by mesoscale activity (Sinha and Richards, 1999; Hughes and Ash, 2001; Sokolov and Rintoul, 2007). Jets tend to form in large-scale flows and are associated to the so-called β effect (Rhines, 1975), where β is the variation in the Coriolis parameter with latitude. The β effect acts on barotropic turbulence and tends to organize the flow in zonal filaments that persist for long periods and are controlled by eddy–mean flow interactions. A similar effect is produced by the topographic gradient when topography slopes in the meridional direction (Thompson, 2010; Thompson and Sallée, 2012; Boland et al., 2012). Moreover, isolated bottom ridges influence jet formation by topographic steering where the current crosses main fracture zones (Gille, 1994). In addition, baroclinic instabilities are associated with eddy growth at the scale of the Rossby radius of deformation, which allows the flow to become more barotropic and, in turn, organizes zonal jets (Panetta, 1993). The release of potential energy in the mean baroclinic flow makes baroclinic jets particularly intense.

The extreme variations in shape of bottom topography are reflected in the very intricate dynamics at the surface, which is highly geographically variable. Despite many efforts over the last decade, these dynamics that are associated with interactions between mean-flow, topography, and eddy field, remain poorly understood. A correct representation of the eddy field is still a major challenge for modelers, mainly in terms of difficulties in determining the most suitable parameterization and the appropriate eddy diffusivity coefficient. In the latest years, considerable work has been devoted to the study of eddy diffusivity to propose more accurate parameterizations. For instance, Shuckburgh et al. (2009) and Griesel et al. (2010) observed some discrepancies between eddy kinetic energy distribution and eddy-induced mixing, which were strongly enhanced near the major submerged ridges. In addition, a reduction in mixing was found in the core of the strongest jets (Marshall et al., 2006; Ferrari and Nikurashin, 2010; Naveira-Garabato et al., 2011; Sallée et al., 2011), and Sallée et al. (2008a, 2011), by analyzing drifter data, underlined the necessity of using higher, non-constant values of eddy diffusivity.

Knowledge about the mechanisms controlling eddy mixing and the distribution of eddy fluxes is of fundamental importance for determining the contribution of the Southern Ocean eddy field to the subduction of water masses. Eddy contribution to water-mass transformation and subduction has often been ignored because of the difficulties in estimating their amount over a broad range of scales from direct measurements. However, Sallée et al. (2006, 2008a) underlined how it can play a relevant role in local mixed layer heat balance, and more recent papers showed that eddy heat fluxes (EHF) play a role in the subduction of water masses, contributing to set the global ocean ventilation and stratification (Karsten and Marshall, 2002b; LaCasce and Isachsen, 2010; Sallée et al., 2010). The main purpose of this study is to analyze the surface geographical variability of eddy momentum and heat fluxes obtained by direct measurements to observe their behavior in the interactions with the mean flow and with the bottom topography and to estimate their influence on water-mass formation. We use more than a thousand Lagrangian surface drifters that simultaneously sample both velocity and temperature, to estimate near-surface EHF. A description of this dataset and the main methods are presented in section two. In section three, pseudo-Eulerian estimates of the mean velocity, the energy fields, and the eddy variability will be presented with a focus on the eddy–mean flow interactions. A description of drifter dispersion is given in section four, before presenting the role of the eddy heat field in water-mass formation in section five. We complete the paper with a discussion of the results and a conclusion.

2. Data and methods

The observations used in this work have been extracted from the surface Global Drifter Program, which contains data from surface drifters equipped with a drogue centered at a 15-m depth, so that their motion follows near-surface currents. Data were selected for the Southern Hemisphere region between 35°S and 65°S, during the time period spanning 1995 to 2006 (Fig.1). The National Oceanic and Atmospheric Administration (NOAA) Atlantic Oceanographic and Meteorological

Laboratory (AOML) processed drifter data based on Hansen and Poulain (1996). Recent studies reported the presence of undiagnosed drogue loss in drifters deployed in the mid-2000s, which might have caused spurious surface current variability computed from these data (Grodsky et al., 2011; Rio et al., 2012; Piecuch and Rynearson, 2012). A loss of drogue can cause velocity bias due to the wind slip of the buoy at the surface. Although we only used drifters reported by AOML as having a 15-m drogue, the dataset could still potentially be contaminated with drifters without drogue. However, our analysis strongly reduces the potential impact of this contamination: first, since in the Southern Ocean the wind slip is evaluated to affect the zonal component of drifters' velocity (Grodsky et al., 2011), our estimates of meridional drifters' displacement and velocity at each location - that is the main focus of this work - is assumed to be entirely due to the ocean flow regime at that location; second, the slip biases the highest frequencies, which we cut off, both in space and time, by applying a pseudo-Eulerian binning method, which we describe below.

The pseudo-Eulerian technique (Davis, 1991a,b) that we applied to the drifter dataset consists of estimating the mean field by averaging the data in geographical bins, and then subtracting it from the data to obtain the fluctuating part. Any binning technique would cause a bias in the calculation of the mean field, and consequently of the eddy component, since drifters' inhomogeneous distribution due to the influence of the Ekman flow leads to the overestimation (underestimation) of velocities in areas of convergence (upwelling) (Hofmann, 1985; Garraffo et al., 2001). To reduce this bias, we sized the bins to 5° × 2.5° (longitude × latitude) to ensure that a significant number of data falls within each bin, providing us with a homogeneous spatial distribution and with statistically significant final estimates (Falco and Zambianchi, 2011; Trani et al., 2011). We next filtered out periods shorter than two days to remove unwanted noise.

2.1 Calculation of eddy momentum fluxes

Eddy momentum and heat fluxes have been obtained from Reynolds decomposition (Muller, 2006):

$U = U(t) + u'(t)$

The fluctuating part, u'(t), contains the whole spectrum of deviations from the mean, from high-frequency waves to interannual fluctuations, and the calculation of the mean may be biased where observations are too sparse and/or auto-correlated (Garraffo et al., 2001). Thus, we filter out high frequencies to avoid aliasing issues (Poulain, 2001) and focus only on mesoscale and larger scales that are the main driver of the transport in the Southern Ocean. A low-pass second order Butterworth filter was applied to individual drifter records of residual speeds and temperatures to remove energy at periods smaller than two days (e.g., tidal and inertial period waves). In addition, trajectories shorter than six days were discarded. The magnitude of error due to uneven data sampling was estimated following Davis (1991a) and Garraffo et al. (2001), and we found that using filtered data led to an average 20% decrease in the sampling error (not shown).

We estimated the impact of seasonality by performing similar decomposition on winter only (April to September) and summer only (October to March) trajectories. Data availability is almost equal for both seasons and is sufficient to guarantee statistical significance. However, interannual variability cannot be investigated because of insufficient data to ensure statistical significance.

The mean field was obtained by averaging all velocity data in each bin for each season:

$$\langle v^k \rangle = \frac{1}{n^k} \sum_{i=1}^{n} v_i^k \quad (1)$$

where the brackets represent the average, n^k is the number of data in the k-th bin. The associated mean kinetic energy (MKE) is computed as

$$\langle MKE^k \rangle = \frac{1}{2} \left| \langle v^k \rangle \right|^2 \quad (2)$$

where $\left| \langle v^k \rangle \right|$ is the amplitude of the mean velocity vector in the k-th bin.

EKE is computed in each bin for each season on the basis of the variances in the zonal and meridional velocity components:

$$\langle EKE^k \rangle = \frac{\langle u\prime \rangle^2 + \langle v\prime \rangle^2}{2} \quad (3)$$

Eddy momentum fluxes can be represented, at a first approximation, by the covariance between zonal and meridional velocity ($\overline{u'v'}$) (Morrow et al.,1994). Positive (negative) values of $\overline{u'v'}$ indicate a northward (southward) flux of zonal momentum. The distribution of positive and negative momentum is associated with convergence and divergence of momentum itself associated with input and removal (resp.) of momentum from the mean flow (see Trani et al., 2011). However, since the ACC shows strong meandering along its path, cross-stream eddy fluxes are not well represented by the covariance term (e.g., Hughes and Ash, 2001).

Hughes and Ash (2001) noted that only the non-divergent component actually interacts with the mean flow. Therefore, by retaining only the non-divergent component (N),we can isolate the actual cross-stream eddy fluxes. We express Reynolds stress divergence as the sum of the eddy kinetic energy gradient and the relative vorticity advection:

$$\vec{F}^{eddy} = -\langle \overrightarrow{V'} \cdot \Delta \overrightarrow{V'} \rangle = \nabla(p+q)/2 + \hat{k} \times J \quad (4)$$

$$\Gamma = -\hat{k} \times J,$$

where $p = \overline{u'u'}$ and $q = \overline{v'v'}$, and

$$J = \overline{w'\varsigma'} = \left[\overline{u'(v'_x - u'_y)}, \overline{v'(v'_x - u'_y)}\right] \quad (5)$$

As long as two-dimensional eddies have been considered horizontally non-divergent ($u'_x + v'_y = 0$), the J component can be expressed in terms of variance and covariance:

$$\Gamma = -\hat{k} \times J = -(s_x + r_y, r_x + s_y) \quad (6)$$

$$s = \frac{\overline{u'u'} - \overline{v'v'}}{2}$$

$$r = \overline{u'v'}.$$

Therefore, Γ, in this calculation, is the flux of eddy vorticity, whose positive (negative) value of zonal component, $(\Gamma = -s_x - r_y)$, represents a northward (southward) eddy vorticity transport.

2.2 Evaluation of drifter dispersion

The influence of topography can be assessed by evaluating drifter displacement relative to the potential vorticity (hereafter PV) field. In the absence of external forcing, a parcel of fluid conserves its PV. Therefore particles tend to drift along PV contours. LaCasce and Speer (1999) demonstrated that this is particularly true in idealized barotropic flows. PV is determined by the vorticity divided by the ocean depth *H*, where the vorticity is the sum of the Coriolis parameter *f*, i.e., the planetary vorticity, and the relative vorticity. However, for large-scale flows at locations far away from the equator, the relative vorticity is small compared to the planetary vorticity, so we neglect it in this study. Ocean depth used in this study has been extracted from the ETOPO5 5-min gridded elevation data provided by the NOAA National Geophysical Data Centre. ETOPO5 was generated from a digital database of land and sea-floor elevations coming from a lot of different sources around the world. This topography field has been smoothed to remove small topographic scales that are irrelevant to the present study and also often too noisy (LaCasce and Speer, 1999). Therefore, data were subsampled at 10 min and filtered using a spectral filtering function, which also simulates the effect of stratification:

$$h_{smooth} = \sum_k \sum_l \hat{h}(k,l) \exp(-\alpha\kappa - ikx - ily) \quad (7)$$

$$\kappa = (k^2 + l^2)^{1/2},$$

where $\hat{h}$ is the Fourier transformed topography, κ is the magnitude of the total wave vector, and α is a smoothing factor with the dimension of length. LaCasce (2000) tested sensitivity to the smoothing factor in North Atlantic topography, assuming smoothing scales of 2 km with $\alpha = 6\times 10^3$m, those of 20 km with $\alpha = 6\times 10^4$m, and those of 200 km with $\alpha = 6\times 10^5$m. He found that the highest value of α led to an extremely noisy field, while the lowest value over-smoothed the field so that contours of

f/H were nearly zonal; therefore, he used $\alpha=6\times 10^4$m as the best compromise. In contrast, in this work, the lowest smoothing factor had to be used, as the topography of the Southern Ocean is much more detailed, so that even the smoothing scale of 20 km led to an extremely noisy field.

Drifter trajectories were subdivided into 20-day segments; this increases the sample number and also ensures a higher statistical significance. The length of the segments is chosen on the basis of the typical Lagrangian time scale. In the Southern Ocean this scale is of a few days (Rupolo, 2007), so the segment length chosen is shorter than that used by LaCasce (2000). However, calculations with segments of 50 days were also performed, revealing no significant differences (not shown). The dataset used here consists of drifter time series of velocities interpolated every 6 h, however we used daily averaged velocities.

Displacements due to the mean and eddy components separately were also evaluated, computing mean velocities at each drifter position and the eddy portion by removing this mean from the drifter velocity. The mean was computed using two different methods as an estimate of the sensitivity of the calculation. First, mean velocity was interpolated at each drifter position using the pseudo-Eulerian mean field with bins of 3° × 1.5° (longitude and latitude, respectively; method similar as LaCasce, 2000). Second, the pseudo-Eulerian mean velocity in each bin, obtained with larger bins of size 5° × 2.5°, was simply removed from all drifter velocities in that bin. The two methods led to very similar results in terms of eddy-induced dispersion, giving us confidence in the statistics performed. The first procedure was ultimately applied because it was associated with smaller bin size.

Following the method described in LaCasce and Speer (1999) and LaCasce (2000), the velocity at each point along a drifter trajectory is projected into axes parallel and perpendicular to the contours defined by the gradient vector of each of the given fields. The resulting quantities are then integrated in time to yield net displacement along and across contours of the field.

Being x(t) and y(t) the time series of the zonal and meridional coordinates of positions along a single segment of trajectory, the displacements at each time are defined as

$\Delta xi=[xi(1)-xi(0), xi(2)-xi(1), xi(3)-xi(2),\ldots]$ (8a)

$\Delta yi=[yi(1)-yi(0), yi(2)-yi(1), yi(3)-yi(2),\ldots]$ (8b)

The projections of the displacements onto the isolines of the 2D-field F(x,y) are computed by taking the cross/dot products with the local gradient of F (in our case F(x,y) is f/H):

$\Delta\zeta\equiv(\Delta x_i,\Delta y_i)\times(\nabla F/|\nabla F|)$ (9a)

$\Delta\eta\equiv(\Delta x_i,\Delta y_i)\cdot(\nabla F/|\nabla F|)$ (9b)

where ζ and η are the coordinates parallel and perpendicular to the isolines, respectively. Since particles can move on closed contours, distances are not conserved after the projection. The mean displacement $M_\zeta(t)$ and dispersion $D_\zeta(t)$ along F(x,y) contours with the relative errors are as follows:

$$M_\zeta(t)=\frac{\sum_i(\zeta_i(t)-\zeta_i(0))}{N}\pm z\left(\frac{D_\zeta(t)}{N-1}\right)^{1/2} \quad (10a)$$

$$D_\zeta(t)=\frac{\sum_i\left(\zeta_i(t)-\zeta_i(0)-M_\zeta(t)\right)^2}{N-1}\left[1\pm z\left(\frac{2}{N-1}\right)^{1/2}\right] \quad (10b)$$

where N is the number of measurements and z=1.96 at the 95% confidence level. The same calculations were conducted using mean and eddy velocity separately.

2.3 EHF and associated water-mass formation

Quantification of EHF needs both velocity and temperature estimations, which are contemporarily available and almost continuously sampled by surface drifters throughout the Southern Ocean. Drifter velocities pertain to a 15-m depth, while the temperature sensor is located 30 cm below the surface. Temperature and velocity measurement can, however, be related to each other since temperature can be considered homogeneous in the first 10–20 m during all seasons in the Southern Ocean (De Boyer Montegut et al., 2004; Dong et al., 2008; Sallée et al., 2008b).

The zonal and meridional eddy components were evaluated using pseudo-Eulerian analysis from the covariance terms of each velocity component with temperature.

Formally, the eddy–mean flow decomposition was applied:

$$\overline{u'T'} = \overline{uT} - \bar{u}\bar{T} \qquad (11a)$$

$$\overline{v'T'} = \overline{vT} - \bar{v}\bar{T} \qquad (11b)$$

where the overbar is the average of all observations in each 5° × 2.5° bin and the prime denotes the deviation from it.

Near-surface EHF was estimated as follows:

$$\rho_0 C_p \overline{v'T'} \qquad (12)$$

where ρ_0 is the mean sea water density taken to be 1025 Kg/m^3, C_p is the specific heat of water at constant pressure taken to be 4000 Jkg^{-1}K^{-1}. High frequencies were removed from velocity and temperature time series as explained in section 2.1, and the seasonal variability has been evaluated by performing the same calculations for winter and summer data, separately. Since the distribution of the EHF shows a non-Gaussian distribution but a distribution rather close to a bi-exponential (as evaluated following Chinn and Gille, 2007), our results based on averages were compared with computations based on medians, which, however, did not show noticeable differences.

Near-surface EHF is then used to evaluate the associated water-mass production in the Southern Ocean. Water-mass production by diapycnal eddy fluxes is evaluated by computing water-mass transformation rate and subduction rate following the formalism introduced by Walin (1982). The transformation rate is the net volume flux of water produced in a given density class. This net production is due to convergence of fluid, which crosses outcropping isopycnals as a consequence of a buoyancy loss or gain (Fig.2). The subduction rate is, more specifically, the volume of water that passes between the ocean mixed layer to the ocean interior. The buoyancy supply needed by a parcel of fluid in the mixed layer to pass into the stratified thermocline, i.e., to subduct, can be provided by air–sea heat exchanges, lateral eddy heat transport, and vertical diffusive processes at the base of the mixed layer. Vertical diffusion was discovered to be important in subtropical regions, where they counteract the effects of the air–sea exchanges (Garrett et al., 1995; Marshall et

al., 1999). In the weakly stratified Southern Ocean, isopycnals are almost vertical, so lateral eddy mixing becomes more relevant (Follows and Marshall, 1994; Marshall, 1997; Sallée et al., 2006). In previous observation-based studies of water-mass formations, the contribution of eddies was estimated from parameterization (Marshall, 1997; Sallée et al., 2006, 2008a, 2010). In this work, we estimated the EHF and their contribution to water-mass formation directly from drifter observations. We also use annual mean climatological fields of mixed layer depth (MLD), mixed layer density, and thermal expansion from Argo profiles. The annual mean transformation rate in a given density class, $\overline{F(\sigma)}$ (m^3/s), is computed following Brambilla et al. (2008):

$$\overline{F(\sigma)} = \frac{1}{\Delta\sigma} \iint dA\,\delta(\sigma'(x,y) - \sigma) f(x,y) \quad (13)$$

where the double integral is the integral of the horizontal density flux f(x, y) in the outcropping area $\sigma=\sigma'$; δ is the delta function; and $\Delta\sigma$ is the step between density classes. The horizontal density flux f(x, y) provided by lateral eddy mixing through the upper mixed layer was defined as

$$f(x,y) = -\alpha \cdot \rho \cdot MLD \cdot div(\overline{\mathbf{v}'T'}) \quad (14)$$

where α is the thermal expansion coefficient, ρ is the density, MLD is the mixed layer depth and $div(\overline{\mathbf{v}'T'})$ is the divergence of the vector field $\overline{\mathbf{v}'T'}$ estimated by drifter data (Eqs. 11a,b and 12). A value of f(x,y) was computed for each of the 5° × 2.5° bins previously defined by the pseudo-Eulerian method. Annual mean climatological fields of α, ρ, and MLD from Argo float observations are linearly interpolated at the center of each bin.

The spatial integral of $\overline{F(\sigma)}$was calculated as follows: first, density classes in steps of 0.1 kg/m^3 have been defined, ranging from 1026.2 and 1027.3 kg/m^3; then $\overline{F(\sigma)}$ has been computed by discretizing Eq. 14:

$$\overline{F(\sigma_i)} = \frac{1}{\Delta\sigma} \sum_{k=1}^{n} f_k\, A_k \Pi(\sigma_k - \sigma_i) \quad (15)$$

where f_k is the horizontal density flux in the k-th bin and A_k and σ_k are the area and the density of the bin, respectively; σ_i is the i-th class density, i.e., the outcropping area, and Π is the Kronecker delta function: $\Pi=1$ if $\sigma_k=\sigma_i$, $\Pi=0$ otherwise.

The result obtained by this calculation represents the volume of water of a given density class, over the whole domain, that undergoes a transformation of density if exposed to the given lateral EHF. Note that positive (negative) values correspond to transformation toward increasing (decreasing) density.

The annual mean formation rate $\overline{M(\sigma)}$ can be derived by the area-integrated annual mean transformation rate using the relation

$$\overline{M(\sigma)} = -\left[\overline{F(\sigma_2)} - \overline{F(\sigma_1)}\right] \quad (16)$$

where σ is comprised between σ_1 and σ_2. $M(\sigma)$ represents the volume flux that accumulates (or is removed) between the isopycnals σ_1 and σ_2, which implies an increase (decrease) in the initial water-mass density. As a consequence, positive values of this quantity indicate a subduction of water from the surface to the ocean interior.

3. Seasonal variability and eddy–mean flow interactions

Geographical structure of winter and summer velocity fields, MKE and EKE distributions are shown in Figs.3 and 4. Interestingly, seasonal fluctuation of velocity and MKE are mostly observed in the vicinity of the main topographic features, i.e., upstream of the Kerguelen Plateau, along the Southeast Indian Ridge, at the crossing of the Macquarie Ridge, in the Pacific Sector on the Eltanin and Udintsev Fracture Zones and at the Drake Passage (Fig. 5a, b). In these regions, winter velocities and MKE are slightly higher.

These regions are associated with the most intense baroclinic jets of the circumpolar belt and are therefore subject to larger variability (e.g., Sallée et al., 2008b). Zhang et al. (2012) suggested that intensification of the ACC jets along the Southeast Indian Ridge could be associated with wind

events. Winter wind intensification could indeed be associated with enhanced meridional Ekman, enhancing the upper-ocean slope of isopycnals, and intensifying the fronts and their vertical velocity shear. Although more subtle, we note that this potential winter intensification of vertical shear and baroclinicity is consistent with winter intensification of EKE in the vicinity of the main topographic features (Fig.4).

The flow regime upstream of the Kerguelen Plateau (between the Ob'Lena Rise at 40°Eand the Kerguelen Plateau at 70°E, see Fig.1) undergoes the largest seasonal variability of velocity and MKE. In this region, the polar front (PF) is subject to particularly strong meridional shift (Orsi et al., 1995; Belkin and Gordon, 1996; Gille, 1999; Moore et al., 1999; Dong et al., 2006; Sokolov and Rintoul, 2009b). We believe that the variability revealed in Figs. 3 and 5 between 40°E and 70°E is mostly related to winter shift in the position of the PF (Moore et al., 1999).

It is expected that eddies and their nonlinear interactions with jets could impact the mean jet–gyre strength, structure, and stability (Thompson, 1978; Dewar and Bane, 1989;Hogg, 1992;Watts et al., 1995); play a role in driving the jet's flanking recirculations (Hogg 1985, 1993); and potentially act as a source of the observed variability. It is, therefore, important to address the question of eddy–mean flow interactions toward our present goal of investigating the impact of eddies on local buoyancy balance and impact on water masses and large-scale circulation. To this aim, we compute the zonal component of the Reynolds stress divergence, ($F_x^{eddy} = -(\overline{u'u'})_x - (\overline{u'v'})_y$) and the northward eddy flux of vorticity, Γ_x, obtained from Eq.6 (Fig. 6). Mean ACC flow position is represented by contours of SSH (Sallée et al., 2008a; Sokolov and Rintoul, 2007, 2009a,b). We note that the ACC is highly filamentary, with branches of the current merging and splitting, very different from a circumpolarly continuous SSH contour (Hughes and Ash, 2001). However, SSH contours represent a useful proxy that follows and links the main filamentary structure of the circumpolar belt (Sallée et al., 2008a; Sokolov and Rintoul, 2007, 2009a,b; Thompson and Sallée, 2012).

The Reynolds stress divergence, F_x, is dominated by the EKE gradient (see Fig. 4 and Fig. 6a), which maximizes downstream of the main topography ridges. The mean field is accelerated in these regions. Overall, we find eastward (i.e., accelerating) eddy force acting on the region of highest eddy kinetic energy, with a westward force to either side of it (Fig. 5). Deriving eddy vorticity from our dataset is challenging because the relatively poor resolution degraded even more when taking gradients. However, we still believe it is worthwhile as being the only direct way to estimate surface eddy forces. Most of the studies tackling eddy forces have taken advantage of altimetry products with their own uncertainty associated with time and space resolution (e.g., Johnson et al., 1992; Morrow et al., 1994; Hughes and Ash, 2001). Eddy vorticity fluxes show that eddies tend to accelerate the mean field above the ridges, while they decelerate it downstream, consistent with Thompson and Sallée (2012). Topographic steering appears therefore as a key player in the exchange of energy between eddies and mean flow in the ACC. Although coarse scale, our results are consistent with the storm track interpretation of jet dynamics described in Williams et al. (2007), as eddies act to both accelerate and decelerate the mean flow in specific regions. They also point to the key role of bottom topography on eddy–mean flow interaction, which must translate into dispersion, mixing, and ultimately cross-stream EHF, which we will investigate in turns in the next sections.

4. Drifter dispersion analysis

Drifter dispersion is investigated in this section in a number of different dynamical regimes, as defined by bottom topography and frontal zone. We define seven regions for their specific characteristics in bottom topography (Fig.7a): East (EKP; 65–115°E) and West (WKP; 0–65°E) of Kerguelen Plateau, East (EMR; 115–160°E), West (WMR; 175–215°E) and over (OCP; 160–175°E) the Campbell Plateau, East of Pacific–Antarctic Ridge (EPAR; 215–255°E), and the Brazil–Malvinas Confluence (BMC; 310–360°E). In addition, each of these sub-domains has been subdivided in three frontal regimes, namely, north of Subantarctic Front (SAF) (hereafter denoted

with the subscript "n" in front of region name), between SAF and PF (hereafter denoted with the subscript "b" in front of region name), and south of PF (hereafter denoted with the subscript "s" in front of region name). Finally, sub-domain with insufficient trajectory segments have been discarded, leaving us with a total of 14 sub-domains with specific dynamical regimes in which we will investigate drifter dispersion.

Eddy dispersion and fluxes are thought to be strongly anisotropic with large dispersion and fluxes along the currents and smaller across the currents. It is, therefore, important to define a coordinate system following the core of the main currents to discriminate between along- and across-stream dynamics. The ACC undergoes large meridional deviation along its paths with significant standing meanders (Orsi et al., 1995; Moore et al., 1999; Sallée et al., 2008a). These meanders appear closely linked to the large-scale structure of bottom topography (see Figs.1 and 7a). As introduced above, the ACC tends to conserve its large-scale PV by following f/H contours and is therefore steered by the major bathymetry structure of the Southern Ocean. This qualitative result can be quantified by computing the mean displacement of drifters across f/H versus the mean meridional displacement (Fig. 7b) in a number of sub-domains (Fig. 7a). Displacements are computed over each 20-day trajectory segments and averaged in each sub-domain. With the exception of the two regions WKP and WMR, the mean displacement across f/H appears small, while meridional displacement is much larger. The regions downstream of the EMR and the BMC undergo very large meridional displacement associated with a strong bathymetry steering by the Indo-Pacific Ridge and the Falkland Plateau. Interestingly, we find that the regions upstream of the largest topographic structure in which the ACC has to circumnavigate are associated with large across f/H displacement. In these regions (WMR and WKP), the topographic obstacles are so great that the flow cannot find a path along f/H and has to climb over topography. These regions are the limits of the f/H coordinate system to distinguish between along- and across-stream dynamics.

We now analyze dispersion due to the mean flow and eddy-induced dispersion over 20-day trajectories in the f/H coordinate system. Dispersion due to the mean flow along f/H is strongly

enhanced in the Kerguelen sectors, where the flow maximizes (Fig. 4; Sallée et al., 2008a). This region of large MKE induces large horizontal shear associated with the mean flow that disperses the drifters. The dispersion due to the mean flow is enhanced in the direction along f/H (Fig.8a) confirming that our choice of an f/H coordinate system is relevant to discriminate between along- and across-stream regimes.

It is interesting to classify the different regions in terms of the bottom topography gradients. The regions close to the Kerguelen Plateau and Pacific–Antarctic Ridge and south of SAF to the west of the Macquarie Ridge (bEKP, sWKP, nWKP, EPAR, sWMR) are associated with larger f/H gradients. Dispersion due to the mean flow is higher and more anisotropic in these regions of elevated f/H gradients. In contrast, dispersion induced by eddies is weaker and more isotropic in the region of elevated f/H gradients. This suggests that steep topography affects more mean flow (e.g., Vallis and Maltrud, 1993), while the eddy field is enhanced in the lee of large topographic features (Sallée et al., 2008a; Thompson and Sallée, 2012) in regions characterized by gentle slopes.

We note that, in the present study, we consider dispersion only over a short period of time to maximize the number of observations. We understand that autocorrelation of the velocity over 20 days might not have converged, preventing the computation of diffusivity estimates (e.g., Griesel et al., 2010; Sallée et al., 2011); it is worth noting that the order of magnitude of zonal and meridional eddy diffusivities in the ACC, on the basis of a subset of the data utilized in the present study, has been recently estimated by Falco and Zambianchi, 2011, as 9×10^7 and $2 \times 10^7 \mathrm{cm}^2\ \mathrm{s}^{-1}$, respectively, using a method introduced by Bauer et al., 1998. For a review on diffusivity estimates see LaCasce, 2008, and more recently, De Dominicis et al., 2012). However, our aim here is to analyze early day dispersion regime caused by different bottom topography configurations. As an illustration of the time series over the first 20 days, in Fig.9, we show the dispersion due to mean flow (Fig.9d–f) and eddies (Fig.9g–i) in the region downstream of the Kerguelen Plateau.

In this particular region, the dispersion induced by mean flow (Fig.9d–f)is anisotropic within the ACC and south of the ACC, while it is more isotropic north of the ACC. The anisotropy is much

more marked for dispersion induced by eddies (Fig.9g–i). In all directions, the mean-induced dispersion increases more rapidly than linearly, with a growth close to quadratic, as one would expect for a unidirectional shear flow (e.g., Taylor, 1953). After 10 days or so, the dispersion due to eddies appears more linear than dispersion due to mean flow. The linear growth is much lower in the across f/H direction than in the along f/H direction, and is consistent with larger dispersion in the along-stream direction that are aligned with f/H contours.

In conclusion, we confirmed with statistical analysis of our dataset that the bottom topography does have a large influence on the mean flow and on dispersion regimes, both induced by mean flow and by eddies. Bottom topography could therefore have important implications for EHF and water-mass formation. We tackle these issues from the same dataset in the next section.

5. EHF impact on water-mass formation, transformation, and subduction

Density classes have been divided, following Sallée et al. (2010), in four main Southern Ocean outcropping water masses: the Subtropical Mode Waters (STMW; 26.2–26.7σT); the light Subantarctic Mode Waters (26.7–26.9σT); the dense Subantarctic Mode Waters (SAMW; 26.9–27.1σT); and the Antarctic Intermediate Waters (AAIW; 27.1–27.3 σT). In this section, we first analyze how eddy heat flux impacts the local heat budget associated with surface layer deep convection in these four water masses (see Eq. 13; e.g., Sallée et al., 2006). Then, we infer subduction rate by averaging eddy heat fluxes over outcrop areas and computing the associated divergence and convergence of volume in a given outcrop (see Eqs. 15 and 16).

5.1 Regional and seasonal variability of the water-mass transformation rate

The volume of water masses associated to lateral EHF on outcropping water masses in different regions of the Southern Ocean are displayed in Figs.10–13 for four different density classes (Eq. 13). Positive (negative) values represent a density increase (decrease). As expected from the eddy

statistics presented in section 3, the major contributions are found upstream and/or downstream the main bottom topographic features: the Kerguelen Plateau (70°E), the Campbell Plateau (170°E), the Eltanin Fracture Zone (220°E), and the Drake Passage (290°E).

The Indian Sector is known to be the main site of SAMW formation, which mainly occurs between the Subtropical Front (STF) and SAF during winter (Talley, 1996; Sloyan and Rintoul, 2001b; Rintoul and England, 2002; Sallée et al., 2006). The combined effect of equatorward Ekman transport and air–sea heat fluxes is thought to be the main driver of SAMW formation there; however, eddy heat diffusion can be equally important in providing further cooling or warming locally (Sallée et al., 2006). Accordingly, EHF is found to lighten a large volume of STMW, north of the Kerguelen Plateau (i.e., prevent deep convection; Fig.10, blue patches), although they provide a major contribution to the densification of mode water between PF and STF, east of the Kerguelen Plateau (i.e., promoting deep conviction; Fig.10, red patches). In contrast, EHF counteracts denser mode water formation directly downstream of the Kerguelen Plateau (Fig. 11), as also noted by Sallée et al. (2006).

Two main regions of densification of large volumes of SAMW were found south of New Zealand, downstream of the Campbell Plateau, and in the Pacific Sector, downstream of the Eltanin Fracture zones (Fig.12), consistent with previous studies (Rintoul and England, 2001; Sallée et al., 2010). However, here we find that this densification occurs in different seasons: to the south of New Zealand, there is a density increase towards denser SAMW in winter (6–8 Sv) directly equatorward of the SAF, while an increase towards lighter SAMW occurs during summer further north (Fig.11c); in the Pacific Sector, a prominent mass flux (8–10 Sv) toward higher densities occurs in summer, while a mass flux toward lower densities can be seen upstream of it and also downstream the Campbell Plateau, though of low intensity (2–4 Sv).

From this analysis, a picture emerges of hotspots of dense water formation in the SAMW density range, which are linked to the bottom topography and extend through Indian and Pacific Oceans. These hotspots of densification are promoting deep convection in these particular regions. We show

here that topography induces EHF important for local mode water production that adds up to the larger scale fluxes induced by air–sea fluxes (Sallée et al., 2006).

In contrast, EHF in the AAIW density class is much weaker, so air–sea heat fluxes would have an outsized role in modifying density at the surface in this layer.

We note that, here, the focus is on the volume of water-mass transformation. This is associated with local buoyancy fluxes affecting the generation of deep convection of the surface mixed layer (e.g., Sallée et al., 2006; Dong et al., 2008). Subduction results from convergence or divergence of the integrated EHF flux over an outcrop (Eqs. 15 and 16), which we tackle below.

5.2 Annual and seasonal mean transformation and subduction rates

EHF strongly contributes to the densification of the lightest waters (STMW). Summer and winter estimates reveal a strong seasonal cycle. This large seasonal cycle is especially marked in the two SAMW density classes marked by an overall densification in both summer and winter, and a strong erosion of SAMW of density around 26.7 σ_T in winter (Fig.14). The large winter erosion is associated with a convergence of water (i.e., subduction) in the light SAMW density class and a divergence of water (i.e., upwelling) in the dense SAMW density class (Fig.15). In summer, the densification to the north and lightening to the south (Fig. 14) lead to a convergence (i.e., subduction) in water around 26.9 σ_T (Fig.15). The densest SAMW (27.0 σ_T) are in part eroded to form AAIW.

It is interesting to note that the order of magnitude of subduction found here is of similar magnitude as total subduction rate estimated in previous studies (e.g., Sallée et al., 2010). Our results highlight, therefore, that any attempt to estimate subduction from a thermodynamic approach has to carefully include lateral eddy-induced fluxes in addition to air–sea buoyancy fluxes.

High eddy-induced subduction of light SAMW occurs in winter, while subduction of STMW and AAIW is mainly enhanced during summer (Table 1). EHF seems to have no great net influence on

dense SAMW formation, but these circumpolar integrated results hide large regional impact as seen in section 5.1.

6. Summary and conclusions

A consistent surface drifter dataset has been used to investigate the impact of mesoscale eddies on Southern Ocean dynamics, from eddy–mean flow interactions to water-mass transformation, and via dispersion regimes. The importance of bottom topography in defining specific regimes has been investigated. The strength of this analysis is to analyze eddy statistics and EHF from the same dataset, and to estimate Southern Ocean surface EHF from direct measurements without any parameterization assumption.

We applied a pseudo-Eulerian technique (Davis, 1991a,b) to surface drifter data collected between 1995 and 2006.Biases in the calculation of the mean field were reduced by choosing the appropriate bin size and filtering out high frequencies. Winter and summer distributions of mean velocity, MKE and EKE are similar, except in regions near the main topographic features. Upstream of the Kerguelen Plateau values of mean velocity and MKE are enhanced during winter, while winter EKE appears to be higher at the Eltanin Fracture Zone. Our results suggest that seasonal variability of these eddy characteristics is partly associated with seasonal meridional shifts of the ACC fronts (Moore et al., 1999).

Eddy–mean flow interactions were evaluated computing the rotational component of the eddy momentum fluxes. Comparing the distributions of the zonal component of the Reynolds stress divergence with the northward eddy flux of vorticity, eddies are found to mostly increase the ACC velocity (see also Morrow et al., 1994). However, maybe more interestingly, we found that eddies work at reducing the speed of the mean current downstream of bottom ridges, in particular the Macquarie Ridge and the Pacific–Antarctic Ridge (Hughes and Ash, 2001; Zambianchi et al., 1999; Falco and Zambianchi, 2011; Thompson and Sallée, 2012).

The link between Southern Ocean surface circulation and bottom topography has been further assessed by analyzing drifter dispersion properties. The mean displacement and dispersion of driftersinduced by mean flow were found to be strongly anisotropic, with the largest dispersion in the direction of the f/H contours. Over the first twenty days, dispersion associated with mean flow is superdiffusive (Berloff and McWilliams, 2002), close to quadratic, as anticipated from a strong shear flow like the ACC (Taylor, 1953). Eddy-induced dispersion is closer to linear with cross-f/H dispersion slower than along-f/H dispersion, as anticipated by a flow steered by bathymetry contours. Indeed, drifters do tend to follow f/H contours, except upstream of very large obstacles that it cannot circumnavigate (e.g., upstream of Kerguelen, upstream of Macquarie Ridge)

These results confirm the strong dependence of the dispersion properties of the ACC on the bottom topography. Consistent with PV dynamics, we find that high gradients are associated with major dispersion due to the mean flow (between fronts and south of PF close to Kerguelen Plateau, Macquarie Ridge, and Pacific–Antarctic Ridge), while slow gradients favor eddy dispersion (north of SAF east of the Macquarie Ridge and Kerguelen Plateau and at the BMC) (Haynes et al., 2007; Dritschel and McIntyre, 2008). Regions of rapid transitions from high to low PV gradients, i.e., downstream the main topographic features, show the tendency of dispersion to be isotropic, which is enhanced in the across-f/H direction. This behavior is particularly evident near the Campbell Plateau, which has been recognized as the principal area of dense SAWM formation in this work as well as in previous studies (Rintoul and England, 2002; Sallée et al., 2010).

The eddy dispersion characteristics described by the surface drifters are associated with eddy-induced heat fluxes impacting water-mass formation, which we can assess from the same dataset. Circumpolar and local rates of water-mass formation induced by EHF have revealed magnitudes comparable to those due to air–sea heat exchanges. Light SAMW (26.7–26.8 σ_T) formation and subduction are enhanced during winter both in global and regional results, with the major contribution in the Indian Sector in agreement with previous studies (Talley, 1996; Sloyan and Rintoul, 2001b; Rintoul and England, 2002; Sallée et al., 2006). Dense SAMW (26.9–27.0 σ_T)

formation shows no significant formation in global estimates while revealing strong regional contributions linked to bottom topography with opposing features: during winter (summer) an increase (decrease) toward higher densities is found south of New Zealand and a decrease (increase) is found in the Pacific center. Local flux in the AAIW density class (27.1–27.3 σ_T) shows almost no subduction, but when summed over the entire Southern Ocean, we find a significant eddy flux contribution to subduction in summer.

The number of Lagrangian data currently available is still not sufficient to explore submesoscale processes that can play a relevant role in the local dynamics (Thompson and Richards, 2011; Schroeder et al., 2012). However, providing both velocity and temperature observations almost in continuous and covering vast areas, drifter data are a precious source to be further exploited in the future. This dataset will be crucial to obtain more detailed measures of the eddy mixing and transport across the ACC, as well as providing hints on how eddy mixing could be influenced by climate variability.

Acknowledgements

This work was partly funded by the CLIMA project of the Italian National Program for Antarctic Research through a PhD scholarship to Marilisa Trani (PhD program in Polar Sciences, Siena University). SVP drifter data have been kindly provided by NOAA's Atlantic Oceanographic and Meteorological Laboratory in Miami. JBS received support from Agence Nationale de la Recherche (ANR), ANR-12-PDOC-0001, as well as from the British Antarctic Survey as a BAS Fellow.

References

Bauer, S., Swenson, M. S., Griffa, A., Mariano, A. J., and Owens, K. 1998. Eddy-mean flow decomposition and eddy-diffusivity estimates in the tropical Pacific Ocean: 1. Methodology. Journal of Geophysical Research-Oceans 103, 30855-30871.

Belkin I.M. and Gordon A.L. 1996. Southern Ocean fronts from the Greenwich Meridian to Tasmania. Journal of Geophysical Research-Oceans 101, 3675–3696.

Berloff P.S., McWilliams J.C. and Bracco A.2002. Material transport in oceanic gyres. Part I: phenomenology. Journal of Physical Oceanography 32, 764–796.

Brambilla E., Talley L. D., and Robbins P. E. 2008. Subpolar Mode Water in the northeastern Atlantic: 2. Origin and transformation. Journal of Geophysical Research 113, C04026.

Boland, E. J. D., A. F. Thompson, E. Shuckburgh, P. H. Haynes, 2012.The Formation of non-zonal Jets over Sloped Topography. Journal of Physical Oceanography 42, 1635–1651.

Bryden H. L. and Cunningham S.A. 2003. How wind-forcing and air-sea heat exchange determine the meridional temperature gradient and stratification for the Antarctic Circumpolar Current. Journal of Geophysical Research 108(C8), 3275.

Chinn B.S. and Gille S.T. 2007. Estimating eddy heat flux from float data in the North Atlantic: the impact of temporal sampling interval. Journal of Atmospheric and Oceanic Technology 24, 923-934.

Davis R.E. 1991a. Observing the general circulation with floats. Deep-Sea Research Part A 38, S531–S571.

Davis R.E. 1991b.Lagrangian Ocean Studies. Annual Review of Fluid Mechanics 23, 43-64.

de Boyer Montégut C., Madec G., Fischer A.,. Lazar A and Iudicone D. 2004. Mixed layer depth over the global ocean: an examination of profile data and a profile-based climatology. Journal of Geophysical Research-Oceans 109, C12003.

De Dominicis, M., Leuzzi, G., Monti, P., Pinardi, N., and Poulain, P. M. 2012.Eddy diffusivity derived from drifter data for dispersion model applications. Ocean Dynamics 62, 1381-1398.

Dewar W. K. and Bane J. M. 1989. Gulf Stream Dynamics: Part I: Mean Flow Dynamics at 73°W. Journal of Physical Oceanography 19, 1558–1573.

Dong S., Gille S.T., Sprintall J. 2007. An Assessment of the Southern Ocean Mixed Layer Heat Budget. Journal of Climate 20, 4425-4442.

Dong, S., Sprintall, J., and Gille, S. 2006. Location of the Antarctic Polar Front from AMSR-E satellite sea surface temperature measurements. Journal of Physical Oceanography 36, 2075–2089.

Dong S., Sprintall J., Gille S. and Talley L. 2008. Southern Ocean mixed- layer depth from Argo float profiles. Journal of Geophysical Research-Oceans 113, C06013.

Dritschel, D. G.And McIntyre M. E. 2008. Multiple Jets as PV Staircases: The Phillips Effect and the Resilience of Eddy-Transport Barriers. Journal of Atmospheric Science, 65, 855–874.

Falco P. and Zambianchi E. 2011. Near-surface structure of the Antarctic Circumpolar Current derived from World Ocean Circulation Experiment drifter data. Journal of Geophysical Research-Oceans116, C05003.

Follows, M. J., and Marshall J.C. 1994. Eddy driven exchange at ocean fronts. Ocean Modelling 102, 5–9.

Ferrari, R., and M. Nikurashin 2010.Suppression of eddy mixing across jets in the southern ocean, Journal of Physical Oceanography 40, 1501–1519.

Garraffo, Z. D., Griffa A., Mariano A.J. and Chassignet E.P. 2001. Lagrangian data in a high resolution numerical simulation of the North Atlantic. II. On the pseudo-Eulerian averaging of Lagrangian data. Journal of Marine Systems 29, 177–200.

Garrett C., Speer K. and Tragou, E. 1995. The relationship between water mass formation and circulation, with application to Phillips' Red Sea model. Journal of Physical Oceanography 25, 1696-1705

Gille, S. T. 1994. Mean sea-surface height of the Antarctic Circumpolar Current from GEOSAT data– method and application. Journal of Geophysical Research 99, 18255–18273.

Gille S.T. 1999. Mass, heat, and salt transport in the southeastern Pacific: A circumpolar current inverse model. Journal of Geophysical Research 104,5191–5210.

Griesel A., Gille S.T., Sprintall J., McClean J.L., LaCasce and Maltrud M.E. 2010. Isopycnal diffusivities in the Antarctic Circumpolar Current inferred from Lagrangian floats in an eddying model. Journal of Geophysical Research-Oceans 115, C06006.

Grodsky, S. A., and R. Lumpkin 2011. Spurious trends in global surface drifter currents, Geophysical Research Letters, 38(L10606).

Hansen D. and Poulain P.M. 1996. Quality control and interpolations of WOCE–TOGA drifter data. Journal of Atmospheric and Oceanic Technology 13**,** 900–909.

Haynes, P. H., D. A. Poet and Shuckburgh E. F.2007. Transport and mixing in kinematic and dynamically consistent flows. Journal of Atmospheric Science 64, 3640–3651.

Hofmann E.E. 1985. The large scale horizontal structure of the Antarctic Circumpolar Current from FGGE drifters. Journal of Geophysical Research-Oceans90, 7087-7097.

Hogg N.G 1985. Evidence for baroclinic instability in the Gulf Stream recirculation. Progress in oceanography 14, 209-229.

Hogg N.G 1992.On the transport of the Gulf Stream between Cape Hatteras and the Grand Banks. Deep Sea Research Part A 39,1231–1246.

Hogg N.G 1993. Toward parameterization of the eddy field near the Gulf Stream. Deep Sea Research Part I 40, 2359–2376.

Hughes C.W. and Ash E.R. 2001. Eddy forcing of the mean flow in the Southern Ocean. Journal of Geophysical Research-Oceans 106, 2713–2722.

Ivchenko V.O., Treguier A.M and Best S.E. 1997. A kinetic energy budget and internal instabilities in the Fine resolution Antarctic Model. Journal of Physical Oceanography 27, 5-22.

Johnson G.C. and Bryden H.L. 1989. On the size of the Antarctic Circumpolar Current. Deep-Sea Research Part A 36, 39–53.

Johnson D.R. Thompson J. D. and Hawkins J.D. 1992. Circulation in the Gulf of Mexico from Geosat altimetry during 1985–1986. Journal of Geophysical Research 97, 2201-2214.

Karsten R. and Marshall J. 2002a. Constructing the residual circulation of the ACC from observations. Journal of Physical Oceanography 32,3315–3327.

Karsten R. and Marshall J. 2002b. Testing theories of the vertical stratification of the ACC against observations. Dynamics of Atmospheres and Oceans 36, 233–246.

LaCasce J.H. 2000. Floats and f/H. Journal of Marine Research, 58, 61–95.

LaCasce, J. H. 2008. Statistics from Lagrangian observations. Progress in Oceanography 77, 1-29.

LaCasce J.H. and Isachsen P.E. 2010. The linear models of the ACC. Progress In Oceanography 84, 139-157.

LaCasce J.H. and Speer K.G. 1999. Lagrangian statistics in unforced barotropic flows. Journal of Marine Research 57, 245–274.

Lu J. and Speer K.G. 2010. Topography, jets, and eddy mixing in the Southern Ocean. Journal of Marine Research 68, 479-502.

Lumpkin R. and Speer K.G. 2007.Global Ocean Meridional Overturning. Journal of Physical Oceanography37, 2550–2562.

Marshall D. 1997. Subducting of water masses in an eddying ocean. Journal of Marine Research55, 201–222.

Marshall J.C., Jamous D. and J. Nilsson 1999. Reconciling thermodynamic and dynamic methods of computation of water-mass transformation rates. Deep-Sea Research Part I 46, 545–572

Marshall J., Nurser A. J. G. and Williams R. G. 1993. Inferring the subduction rate and period over the North Atlantic. Journal of Physical Oceanography 23, 1315–1329.

Marshall J. and Radko T. 2003: Residual mean solutions for the Antarctic Circumpolar Current and its associated overturning circulation. Journal ofPhysical Oceanography 33,2341–2354.

Marshall J., Shuckburgh E., Jones H. and Hill C.2006. Estimates and implications of surface eddy diffusivity in the Southern Ocean derived from tracer transport. Journal of Physical Oceanography 36, 1806–1821.

McCartney M. S. 1977.Subantarctic mode water. In: M. V. Angel (Eds), A Voyage of Discovery: George Deacon 70th Anniversary Volume (supplement to Deep-Sea Research). Pergamon Press, pp 103–119.

Moore J., Abbott M. and Richman J. 1999. Location and dynamics of the Antarctic Polar Front from satellite sea surface temperature data. Journal of Geophysical Research 104, 3059–3073.

Morrow R., Coleman R., Church J. and Chelton D. 1994. Surface eddy momentum flux and velocity variances in the Southern Ocean from Geosat altimetry. Journal of Physical Oceanography 24, 2050–2071.

Munk, W.H. and Palmen E. 1951.Note on dynamics of the Antarctic Circumpolar Current. Tellus 3, 53–55.

Muller P. 2006. The equations of oceanic motions. Cambridge University Press.

Naveira-Garabato A.C., Ferrari R. and Polzin K.L. 2011. Eddy stirring in the Southern Ocean. Journal of Geophysical Research 116, 1978–2012.

Olbers D., Borowski D., Völker C. and Wölff J.O. 2004. The dynamical balance, transport and circulation of the Antarctic Circumpolar Current. Antarctic Science 16,439-470.

Orsi A.H., Whitworth T.W. III and Nowlin W.D. Jr. 1995. On the meridional extent and fronts of the Antarctic Circumpolar Current. Deep Sea Research Part I 42, 641–673.

Panetta R.L. 1993. Zonal jets in wide baroclinically unstable regions: persistence and scale selection. Journal of Atmospheric Science 50, 2073– 2106.

Piecuch, C. G. and T. A. Rynearson, 2012.Quantifying Dispersal and Connectivity of Surface Waters Using Observational Lagrangian Measurements. Journal of Atmospheric and Oceanic Technology 29, 1127–1138.

Poulain P.-M. 2001. Adriatic Sea surface circulation as derived from drifter data between 1990 and 1999. Journal of Marine Systems29, 3–32.

Rhines P.B. 1975.Waves and turbulence on a beta-plane. Journal of Fluid Mechanics 69, 417-443.

Rintoul S. and England M. 2002. Ekman transport dominates air-sea fluxes in driving variability of subantarctic mode water. Journal of Physical Oceanography 32, 1308–1321.

Rio, M.-H., 2012. Use of altimeter and wind data to detect the anomalous loss of SVP-type drifter's drogue. Journal of Atmospheric and Oceanic Technology29, 1663–1674.

Rupolo V. 2007. A lagrangian-based approach for determining trajectories taxonomy and turbulence regimes. Journal of Physical Oceanography 37,1584–1609.

Sallée J.B., Wienders N., Speer K. and Morrow R. 2006. Formation of Subantarctic mode water in the southeastern Indian Ocean. Ocean Dynamics 56, 525-542.

Sallée J.B., Speer K., Morrow R. and Lumpkin R. 2008a. An estimate of Lagrangian eddy statistics and diffusion in the mixed layer of the Southern Ocean. Journal of Marine Research 66, 441-463.

Sallée, J., Speer, K. & Morrow, R., 2008b. Response of the Antarctic Circumpolar Current to atmospheric variability. Journal of Climate 21, 3020–3039.

Sallée J.- B., Speer K., Rintoul S., and Wijffels S. 2010. Southern Ocean thermocline ventilation Journal of Physical Oceanography 40, 50–529.

Sallée, J.B., Speer, K. and Rintoul, S.R 2011. Mean-flow and topography control on surface eddy-mixing in the Southern Ocean. Journal of Marine Research, 69, 753-777.

Schroeder K., J. Chiggiato, A. C. Haza, A. Griffa1, T. M. Özgökmen4, P. Zanasca, A. Molcard, M. Borghini, P. M. Poulain, R. Gerin, E. Zambianchi, P. Falco, C. Trees 2012. Targeted Lagrangian sampling of submesoscale dispersion at a coastal frontal zone. Geophysical Research Letters 39 (11), L11608.

Shuckburgh E., Jones E., Marshall J. and Hill C. 2009. Understanding the regional variability of eddy diffusivity in the Pacific sector of the Southern Ocean. Journal of Physical Oceanography 39, 2011–2023.

Sloyan B.M. and Rintoul S.R. 2001a.The Southern Ocean limb of the global deep overturning circulation. Journal of Physical Oceanography 31,143–173.

Sloyan, B.M. and Rintoul S.R. 2001b. Circulation, renewal, and modification of Antarctic Mode Water and Intermediate Water. Journal of Physical Oceanography 31, 1005–1030.

Sinha B. and Richards K. 1999. Jet structure and scaling in the Southern Ocean. Journal of Physical Oceanography 29(6). 1143–1155.

Sokolov S. and Rintoul S.R. 2007. Multiple jets of the Antarctic Circumpolar Current south of Australia. Journal of Physical Oceanography 37, 1394-1412.

Sokolov S. and Rintoul S. R. 2009a. Circumpolar structure and distribution of the Antarctic Circumpolar Current fronts: 1. Mean circumpolar paths. Journal of Geophysical Research 114, C11019.

Sokolov S. and Rintoul S. R. 2009b. Circumpolar structure and distribution of the Antarctic Circumpolar Current fronts: 2. Variability and relationship to sea surface height. Journal of Geophysical Research 114, C11019.

Stammer D. 1998. On eddy characteristics, eddy transports, and mean flow properties. Journal of Physical Oceanography 28, 727–739.

Taylor G.I. 1953. Dispersion of soluble matter in solvent flowing slowly through a tube. Proceedings of the Royal Society of London A219, 186-203.

Talley L. D. 1996.Antarctic Intermediate Water in the South Atlantic. In: G. Wefer et al. (Eds): The South Atlantic: Present and Past Circulation. Springer, pp. 219–238.

Thompson R.1978. Reynolds stress and deep counter-currents near the Gulf Stream. Journal of Marine Research 36, 611-615.

Thompson, A.F., 2010. Jet formation and evolution in baroclinic turbulence with simple topography. Journal of Physical Oceanography, 40, 257-278.

Thompson, A.F. & J.B. Sallée, 2012. Jets and topography: Jet transitions and the impact on transport in the Antarctic Circumpolar Current. Journal of Physical Oceanography, 42, 956-972.

Thompson, A. F., and K. J. Richards 2011.Low frequency variability of Southern Ocean jets .Journal of Geophysical Research, 116, C09022.

Trani M., Falco P. and Zambianchi E. 2011.Near-surface eddy dynamics in the Southern Ocean. Polar Research 2011, 30, 11203.

Vallis,J.K, and M.E. Maltrud 1993. Generation of mean flow and jets on a beta-plane and over topography. Journal of Physical Oceanography, 23, 1346-1362.

Walin G. 1982.On the relation between sea-surface heat flow and thermal circulation in the ocean. Tellus 34, 187–195.

Watts D.R., Tracey K.L., Bane J.M. and Shay T.J. 1995.Gulf Stream path and thermocline structure near 74°W and 68°W. Journal of Geophysical Research 100, 18291–18312.

Williams R.G., Wilson C. and Hughes C.W. 2012.Ocean and Atmosphere Storm Tracks: The Role of Eddy Vorticity Forcing. Journal of Physical Oceanography 37, 2267-2289.

Zambianchi E., G. Budillon, P. Falco, and G. Spezie 1999. Observations of the Dynamics of the Antarctic Circumpolar Current in the Pacific Sector of the Southern Ocean. Oceanography of the Ross Sea Antarctica, 37-50.

Zhang L.L., Sun C. and Hu D.X. 2012. Interannual variability of the Antarctic Circumpolar Current strength based on merged altimeter data. Chinese Science Bulletin 57, 2015-2021.

Figure Captions

Fig.1 World Ocean Circulation Experiment Surface Velocity Program drifter trajectories (gray lines) from 1995 to 2006 in the selected area from 70°S to 35°S around the globe. Main features of bottom topography are superimposed (black contours).

Fig.2 Schematic description of water-mass transformation and formation. a) Density change of a surface water mass toward the next higher density; b) convergence of water-mass transformation, which leads to subduction from the surface mixed layer into the ocean interior. It is referred to as a positive formation; c) divergence of water-mass transformation, which leads to obduction from the ocean interior to the surface mixed layer. It is referred to as a negative formation. (From Brambilla et al., 2008).

Fig. 3 Winter (a) and summer (b) mean velocity fields (red arrows) superimposed to the respective MKE fields (color palette). Black contours highlight the main topographic features.

Fig. 4 Winter (a) and summer (b) EKE fields with superimposed black contours highlighting the main topographic features.

Fig. 5 Meridional winter (blue lines with point markers) and summer (red lines with star markers) longitudinal averages at ACC latitudes from 45°S to 60°S of a) absolute velocity, b) MKE and c) EKE. Positions of the main bottom topographic features are indicated below the bottom panel.

Fig. 6 a) Zonal component of the Reynolds stress divergence (F_x^{eddy})and b) northward eddy flux of vorticity (Γ_x)with superimposed SSH contours (black lines).

Fig. 7 a) f/H field with the superimposed SAF and PF. Red lines delimitate the sub-domains used for the trajectory dispersion analysis: West Kerguelen Plateau (WKP), East Kerguelen Plateau (EKP),West Macquarie Ridge (WMR), East Macquarie Ridge (EMR), On Macquarie Ridge (OMR),East Pacific–Antarctic Ridge (EPAR), Brazil–Malvinas Confluence (BMC). b) Mean meridional displacement versus mean displacement of drifters across f/H in each region: areas north of SAF, south of PF, and between SAF and PF are indicated respectively by the blue, green and red dots and by the letters n, s and b before the acronym of the region.

Fig. 8 a) Mean dispersion along f/H versus across f/H, and b) eddy dispersion along f/H versus across f/H computed in each region. Areas north of SAF, south of PF, and between SAF and PF are indicated respectively by the blue, green and red dots and by the letters n, s and b before the acronym of the region (see fig.7 for acronyms' definitions).

Fig. 9 Drifters trajectories downstream of the Kerguelen Plateau: a) on the northward side of the SAF; b) between the SAF and PF; c) south of the PF.

Upper panel of each figure: f/H field with superimposed drifter trajectory segments and ACC fronts; bottom panels: mean (left side graphs of each figure) and dispersion (right side graphs of each figure) due to total velocity, mean and eddy components relative to f/H (along=diamonds, across=black dots) and geographical coordinates (zonal=black lines, meridional=dashed lines); Small dotted lines in the graphs indicate the 95% confidence limits for the mean and dispersion relative to the f/H field.

Fig. 10a),b), and c) Regional distribution of the annual (top panel), winter (central panel), and summer (bottom panel) water-mass transformation induced by the eddy heat field for the STMW density class. Red lines represent the main ACC fronts.

Fig. 11a),b), and c) Regional distribution of the annual (top panel), winter (central panel), and summer (bottom panel) water-mass transformation induced by the eddy heat field for the light SAMW density class. Red lines represent the main ACC fronts.

Fig. 12a),b), and c) Regional distribution of the annual (top panel), winter (central panel), and summer (bottom panel) water-mass transformation induced by the eddy heat field for the dense SAMW density class. Red lines represent the main ACC fronts.

Fig. 13a),b), and c) Regional distribution of the annual (top panel), winter (central panel), and summer (bottom panel) water-mass transformation induced by the eddy heat field for the AAIW density class. Red lines represent the main ACC fronts.

Fig. 14 Annual (top panel), winter (central panel), and summer (bottom panel) water-mass transformations induced by the eddy heat field for each density class for the whole domain.

Fig. 15 Annual (top panel), winter (central panel), and summer (bottom panel) water-mass subduction induced by the eddy heat field for each density class for the whole domain.

Table 1. Winter and summer subduction rates over the whole domain of the main Southern Ocean water masses: Subtropical Mode Water (STMW), light Subantarctic Mode Water (SAMWlight), dense Subantarctic Mode Water (SAMWdense), and Antarctic Intermediate Water (AAIW).

	WINTER	SUMMER
STMW	-2 Sv	16 Sv
SAMW light	20 Sv	5.3 Sv
SAMW dense	-1 Sv	2.1 Sv
AAIW	6.8 Sv	18 Sv

Table 1

Figure 1 b&w

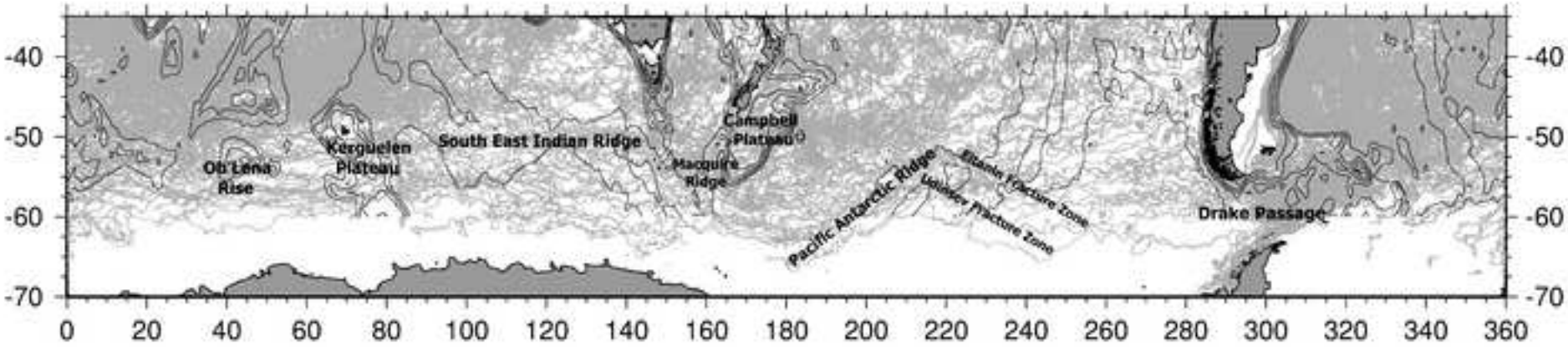

Figure 2

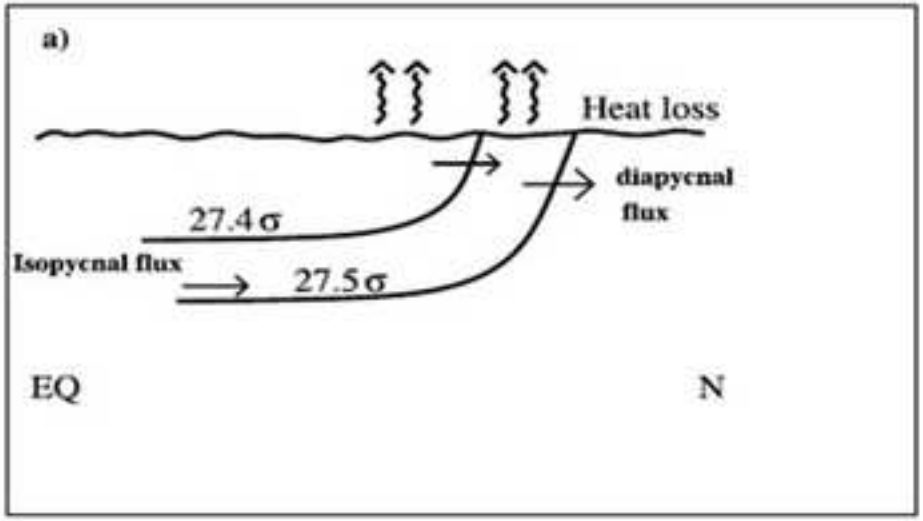

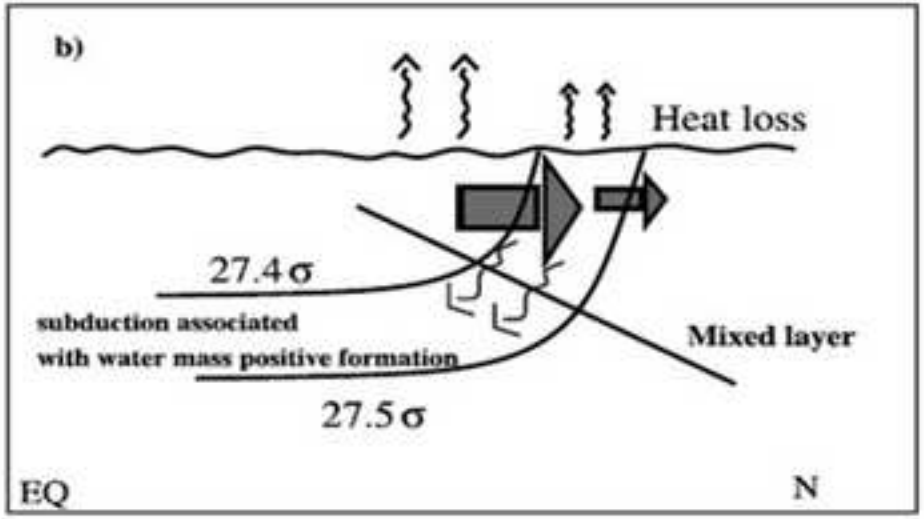

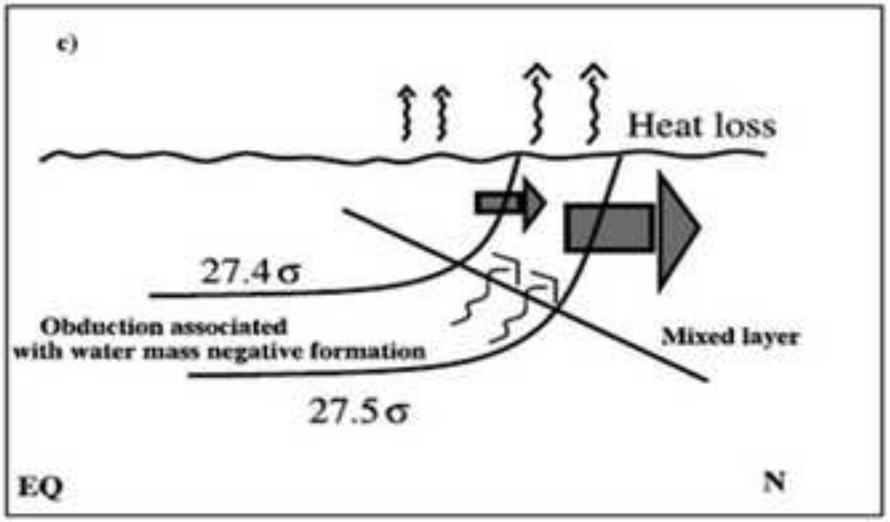

Figure 3a b&w

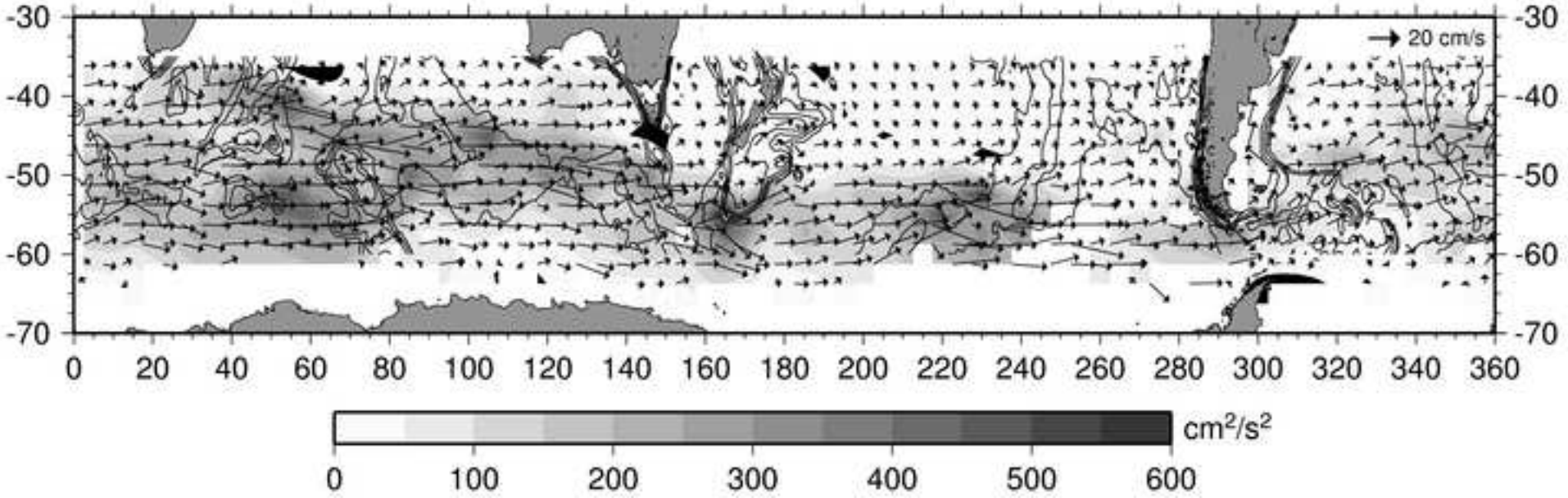

Figure 3b b&w

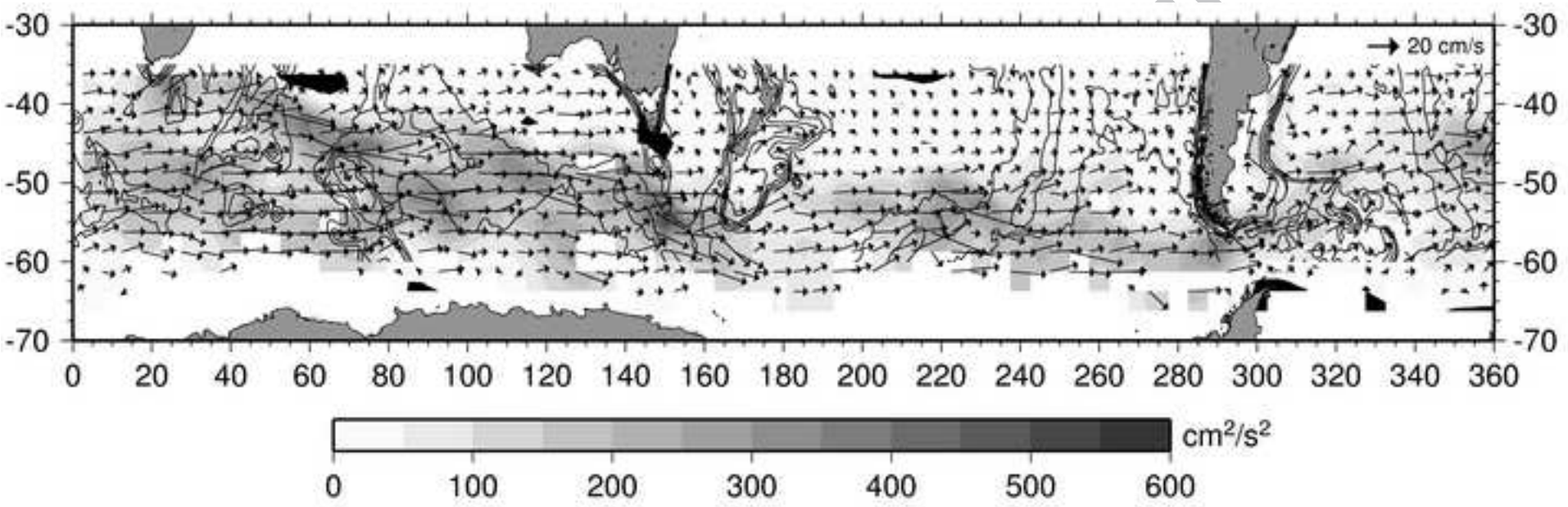

Figure 4a b&w

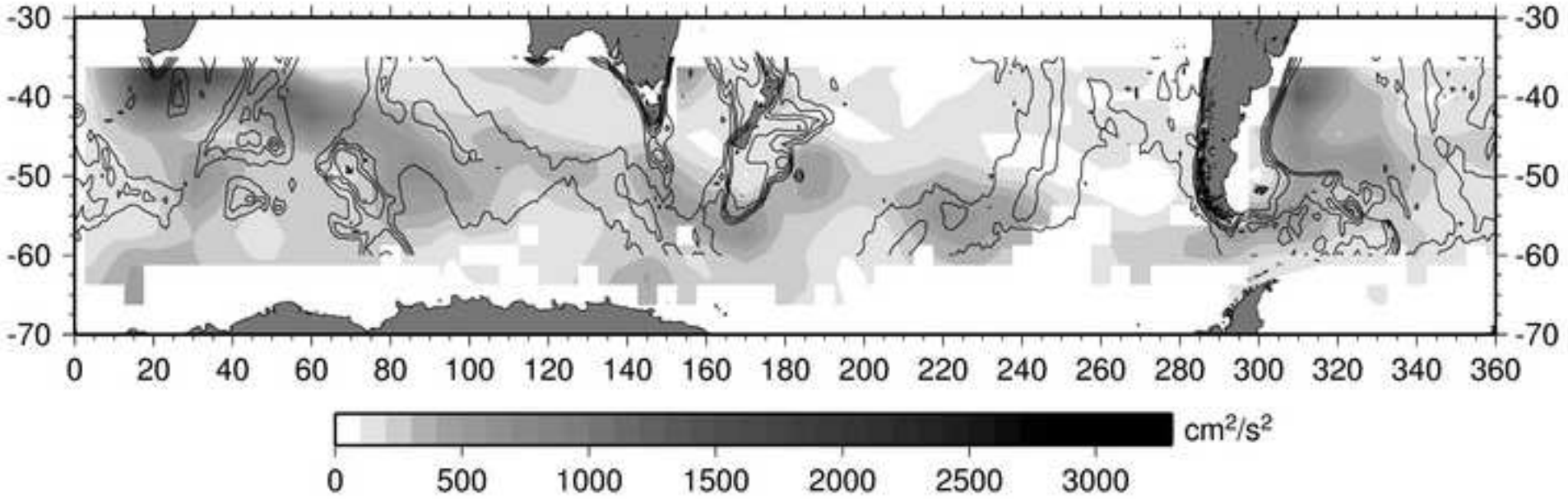

Figure 4b b&w

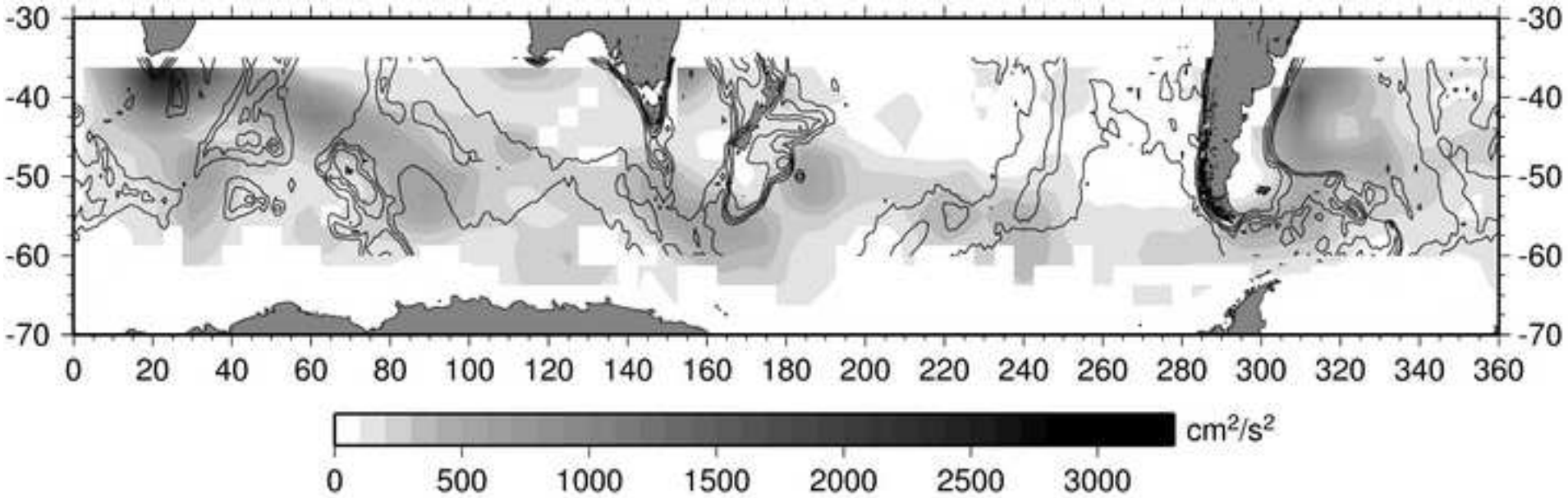

Figure 5 b&w

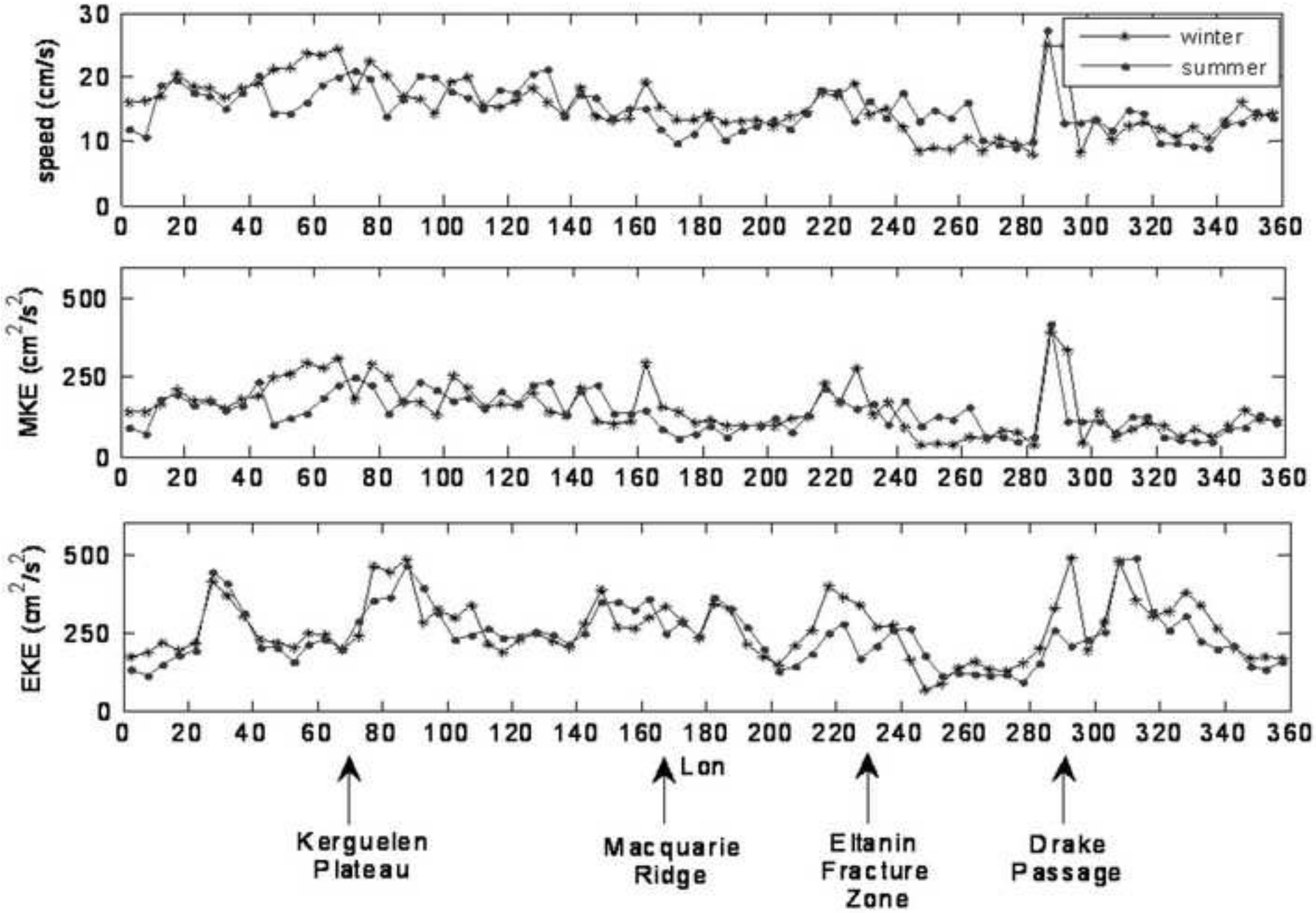

Figure 6a b&w

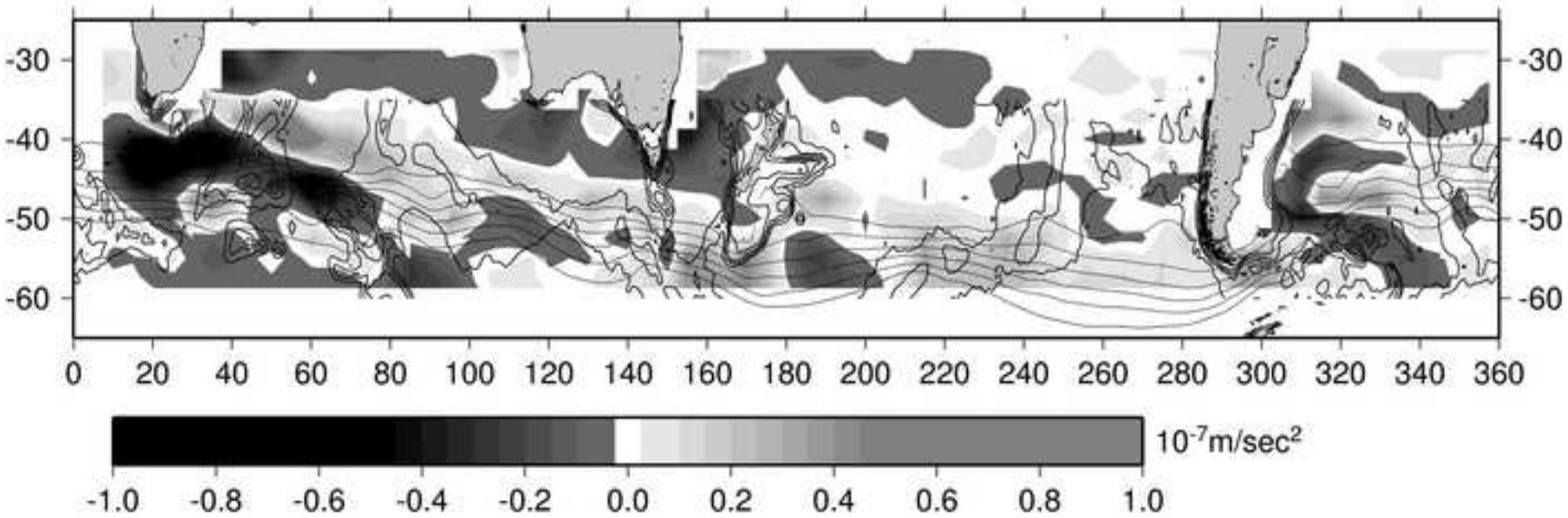

Figure 6b b&w

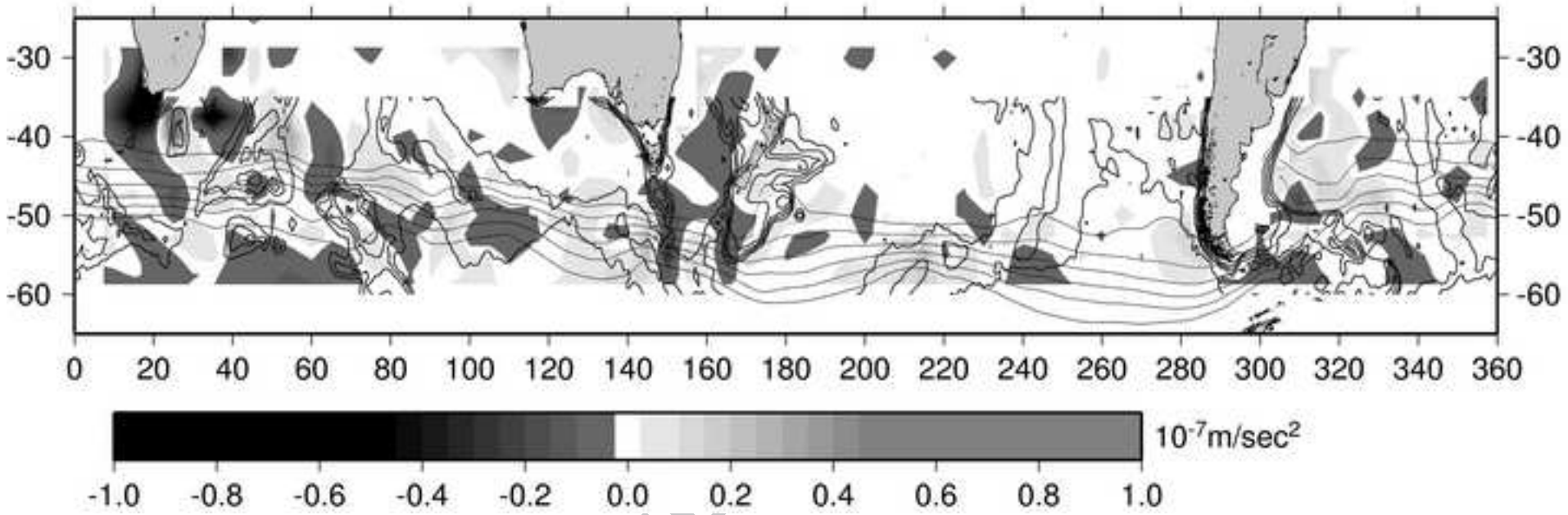

Figure 7a b&w

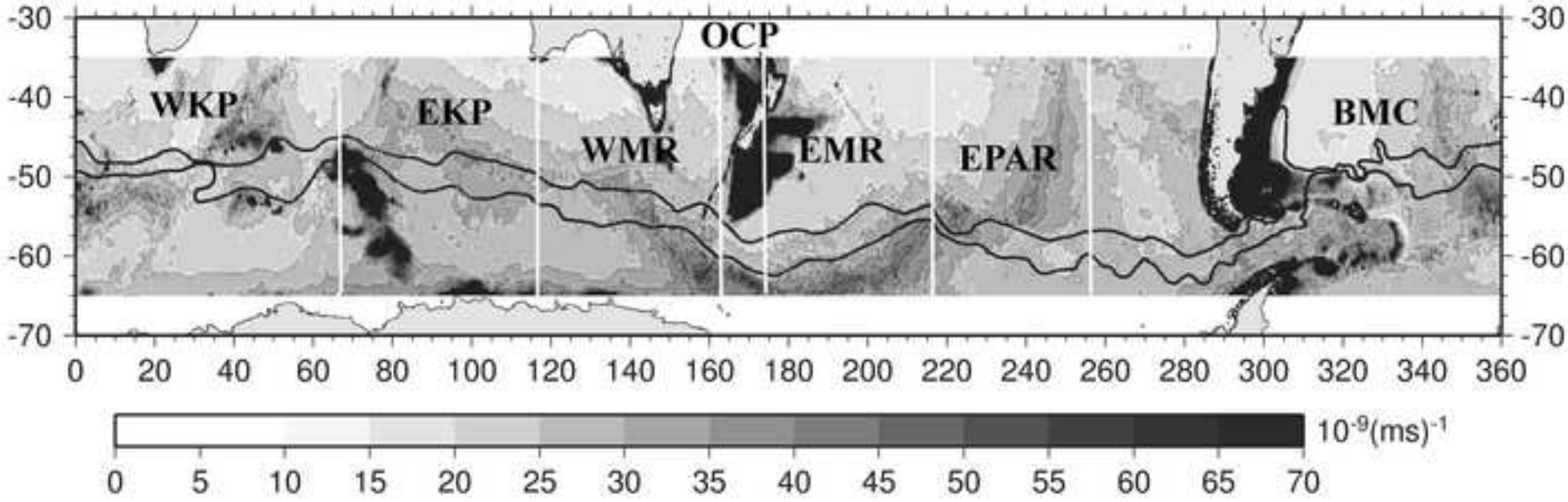

Figure 7b b&w

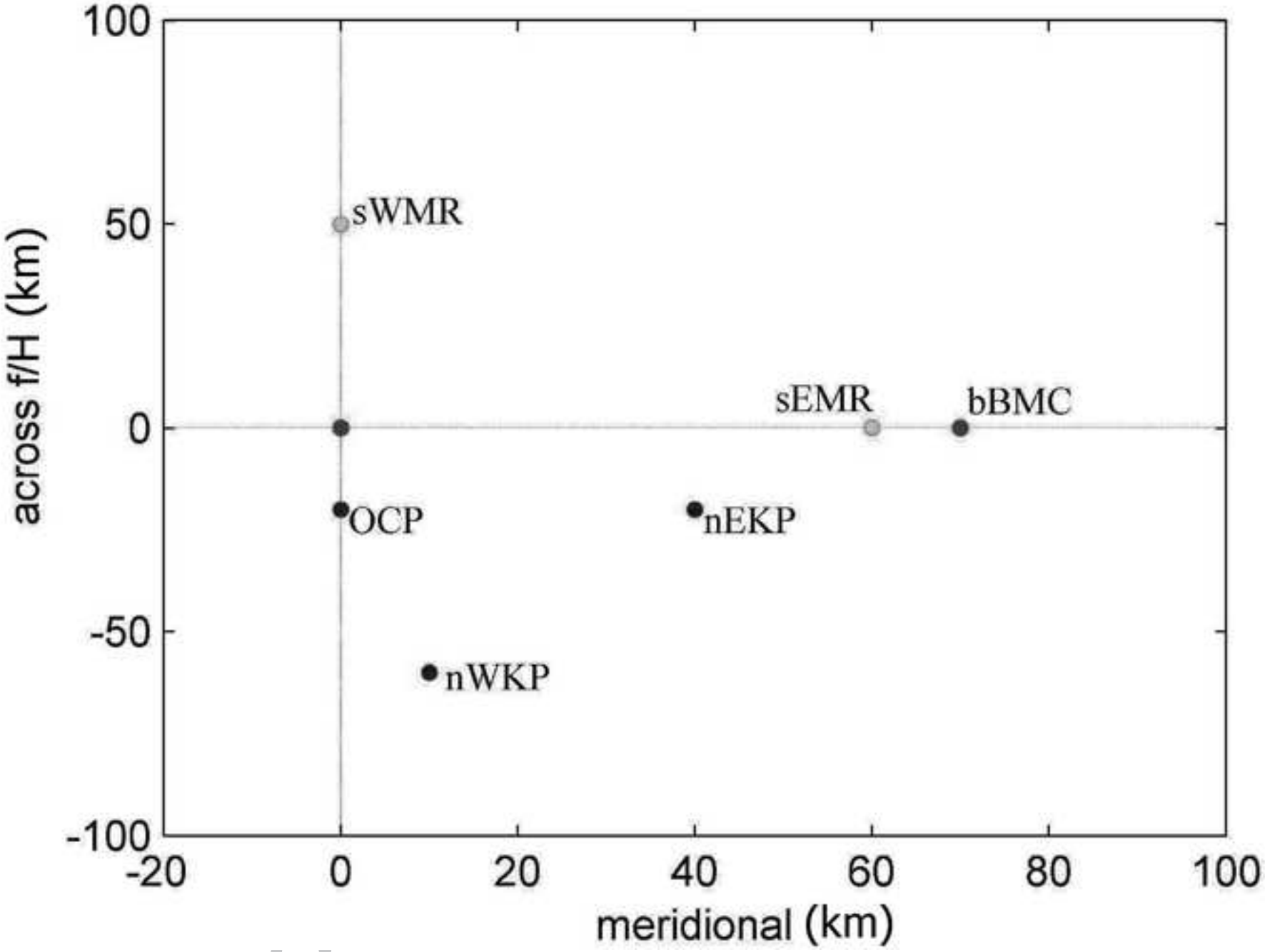

Figure 8a b&w

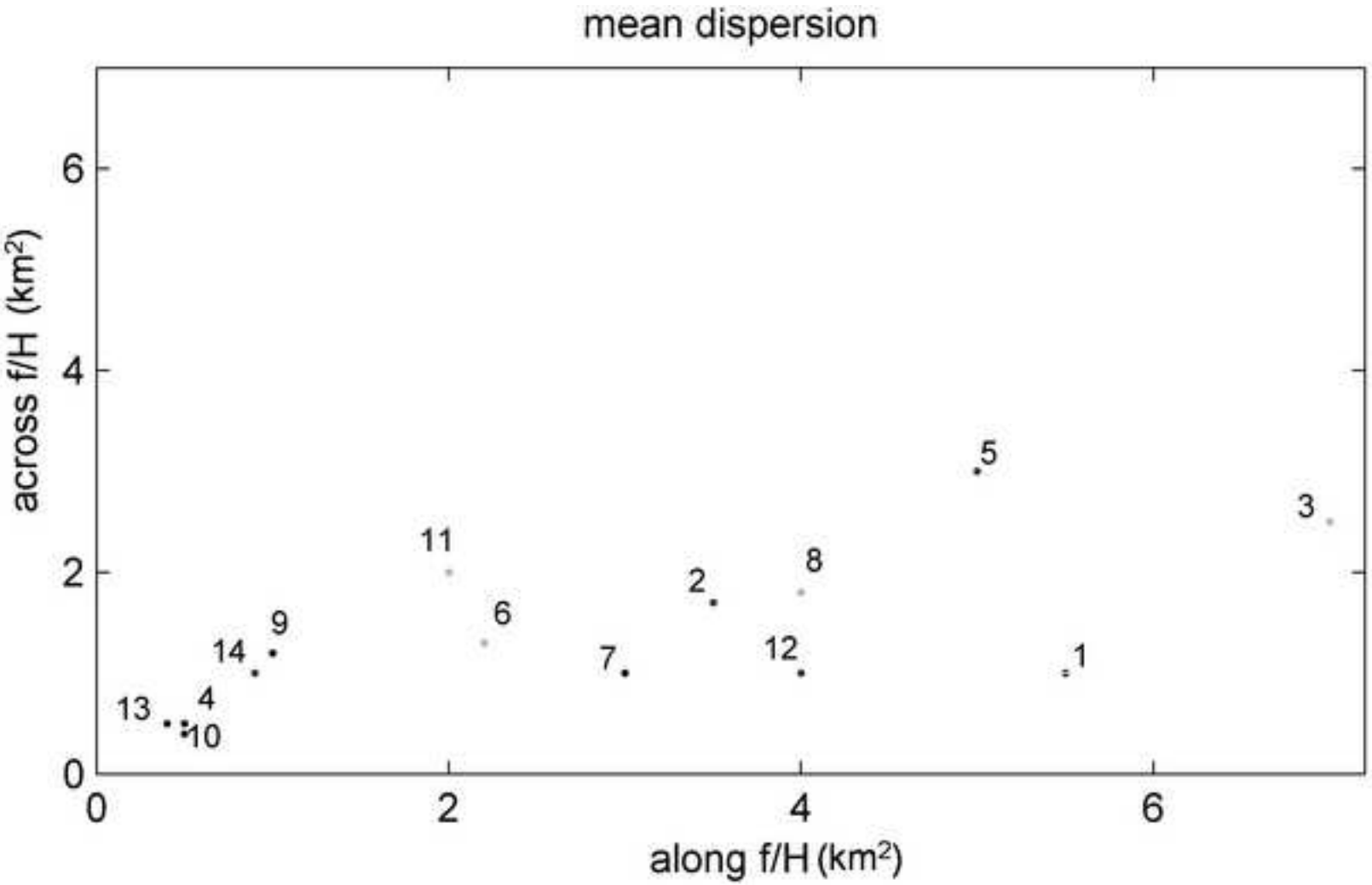

Figure 8b b&w

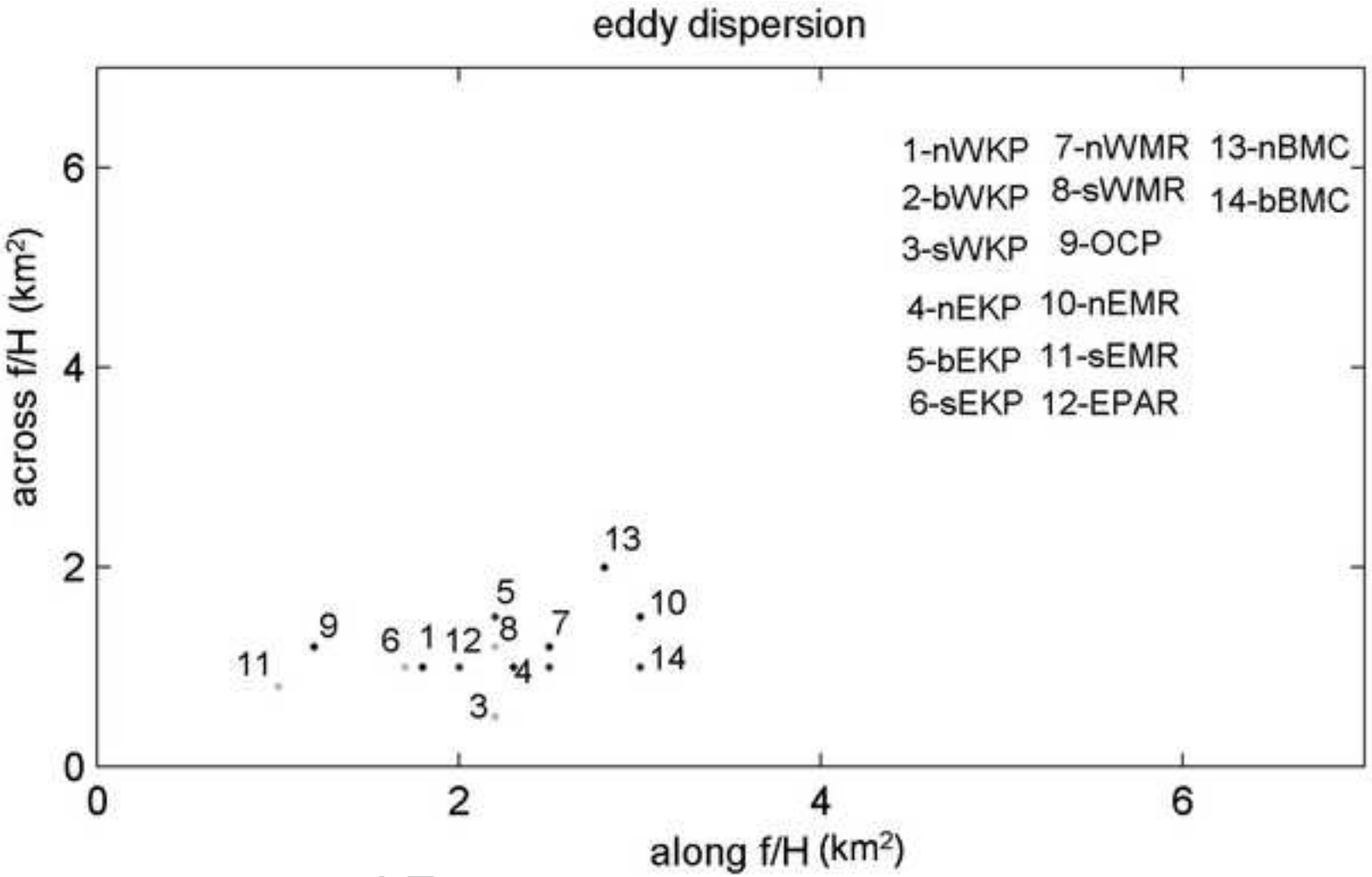

Figure 9 b&w

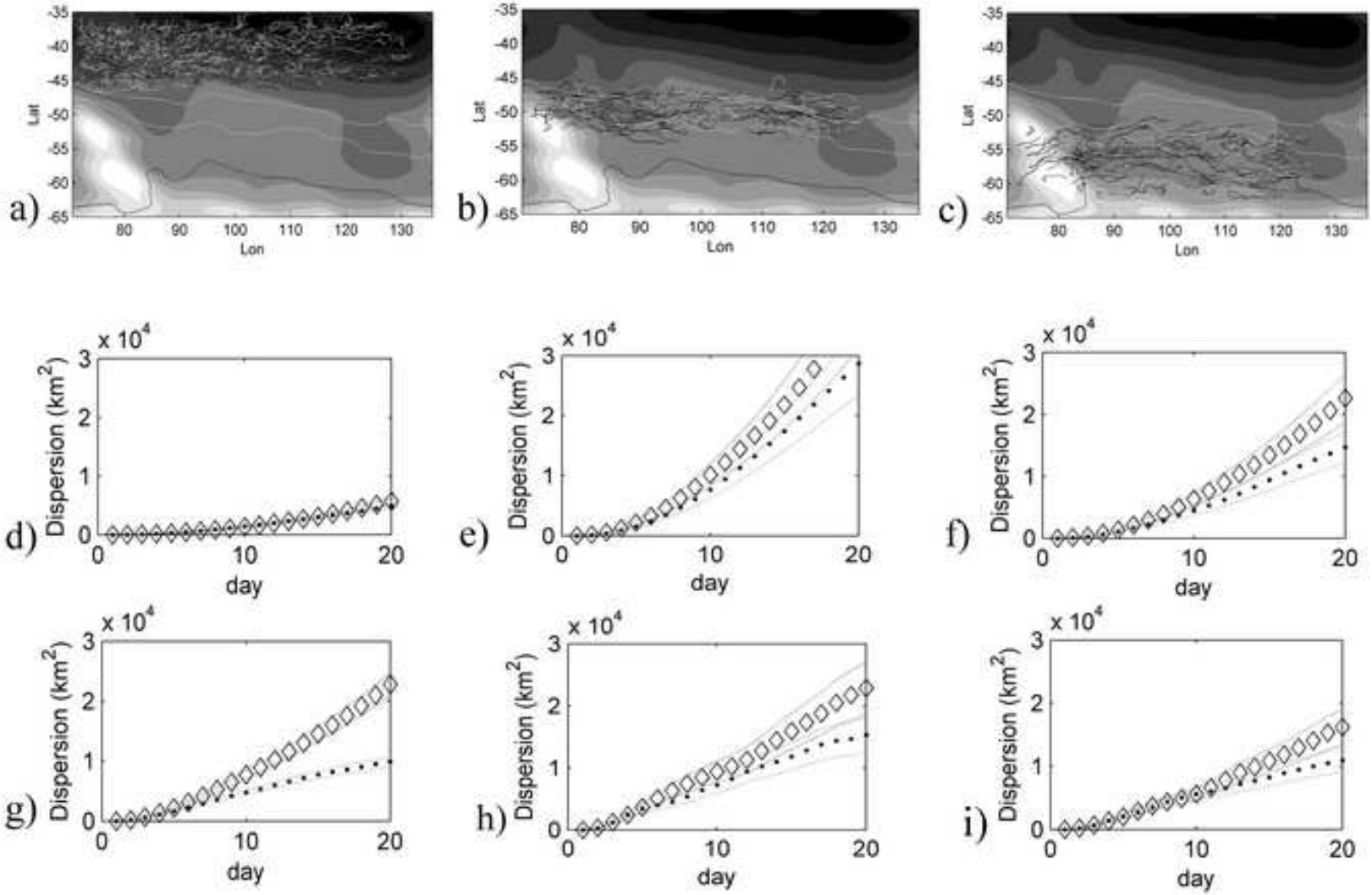

Figure 10 b&w

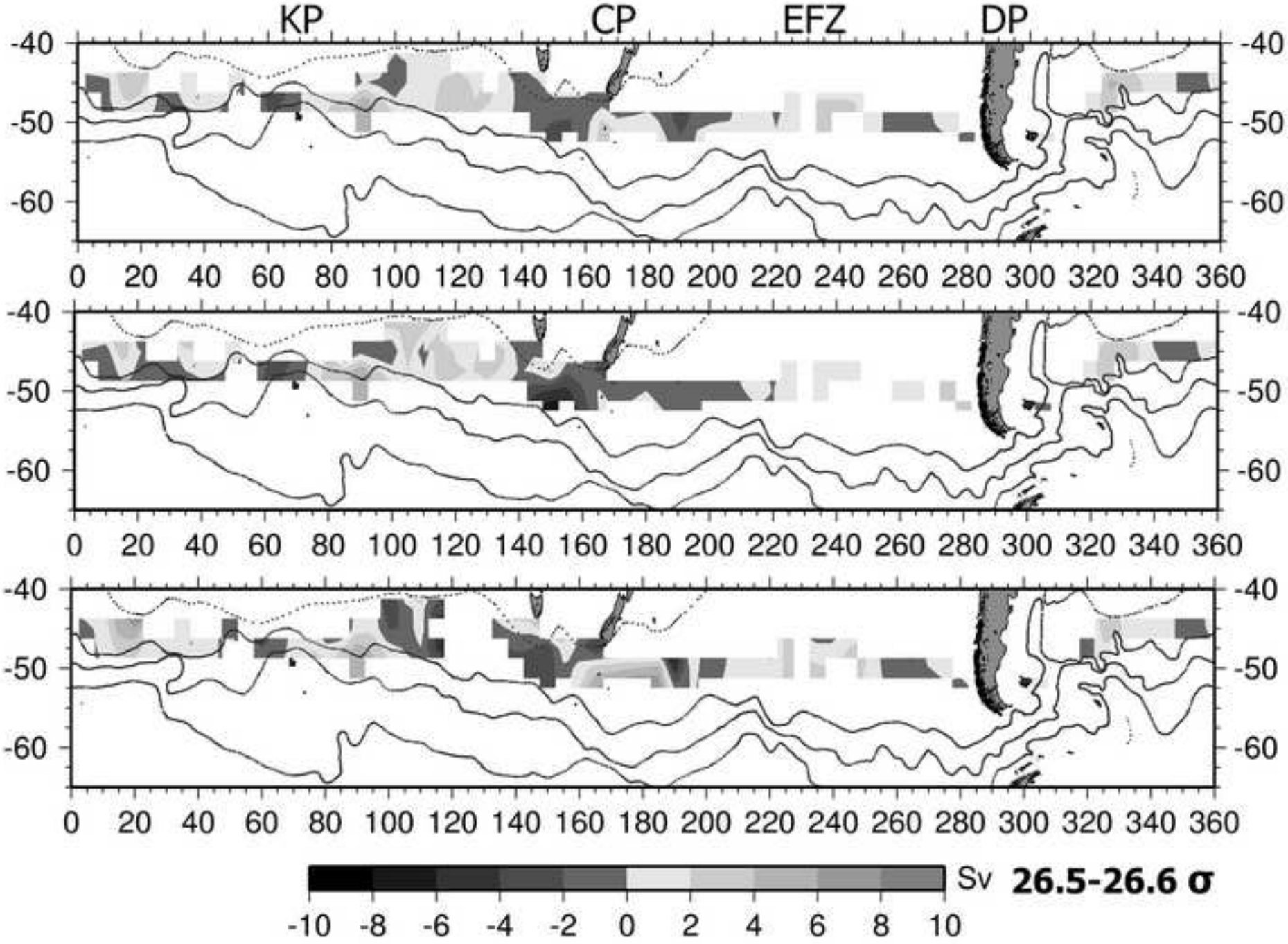

Figure 11 b&w

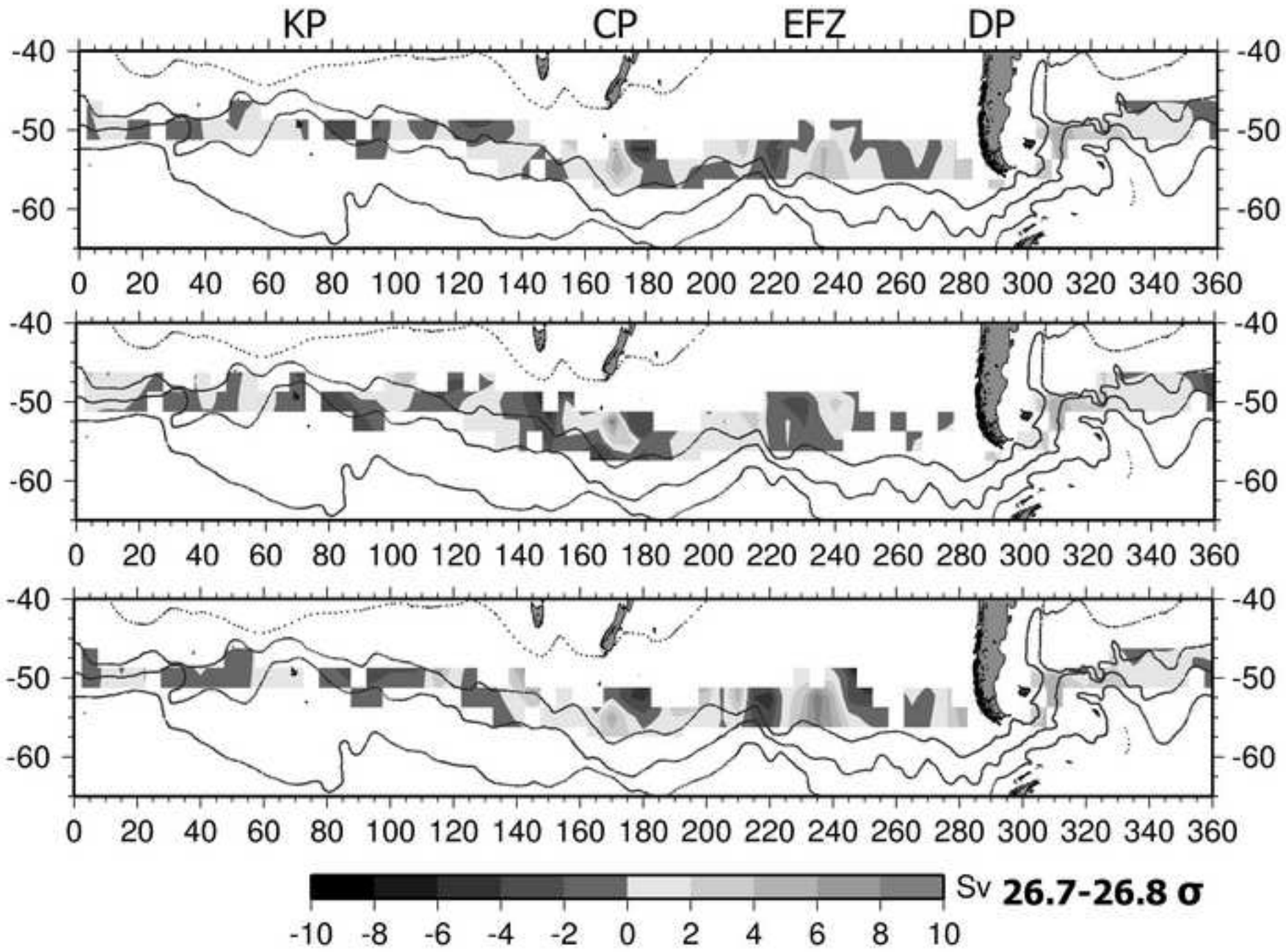

Figure 12 b&w

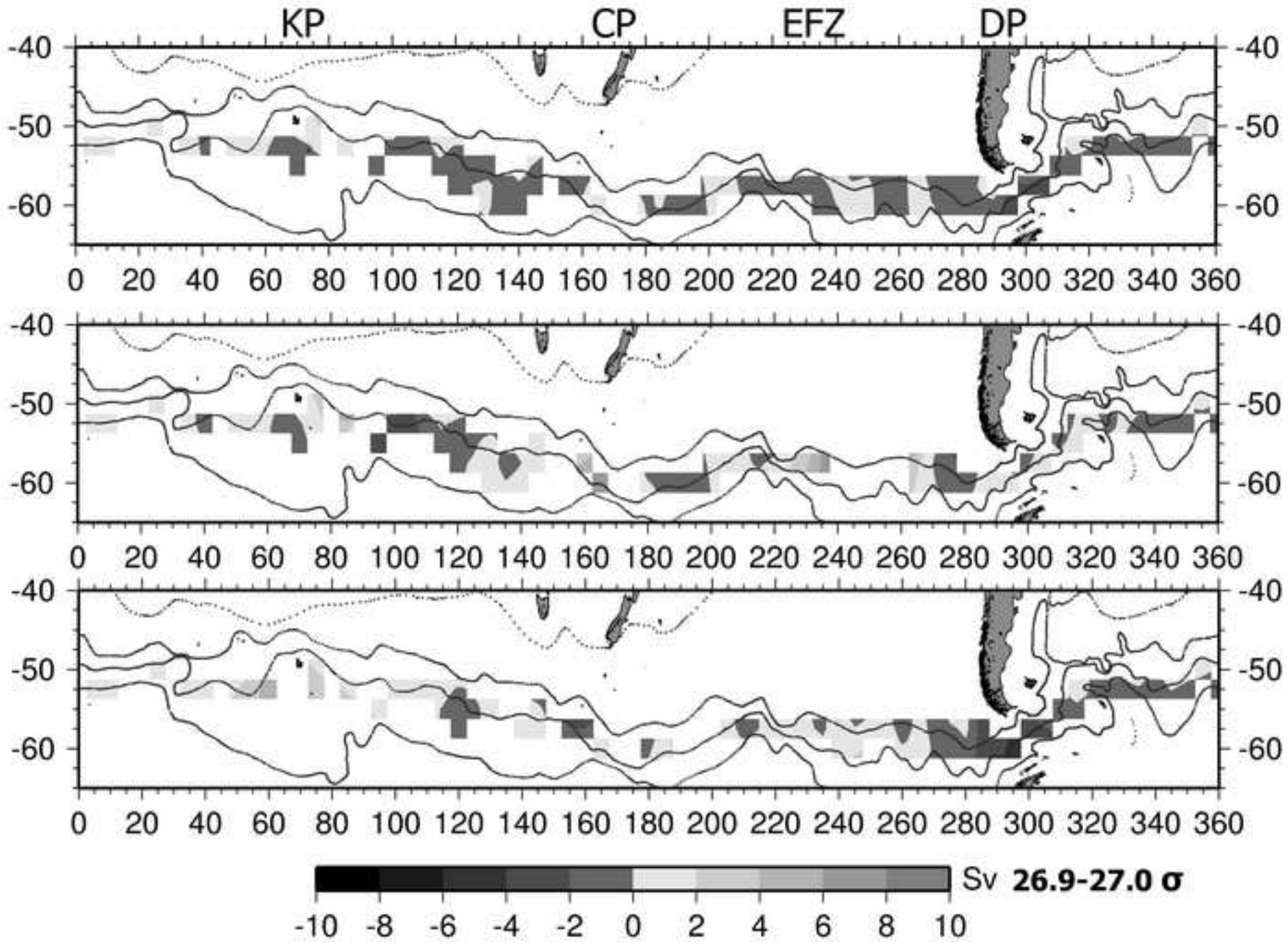

Figure 13 b&w

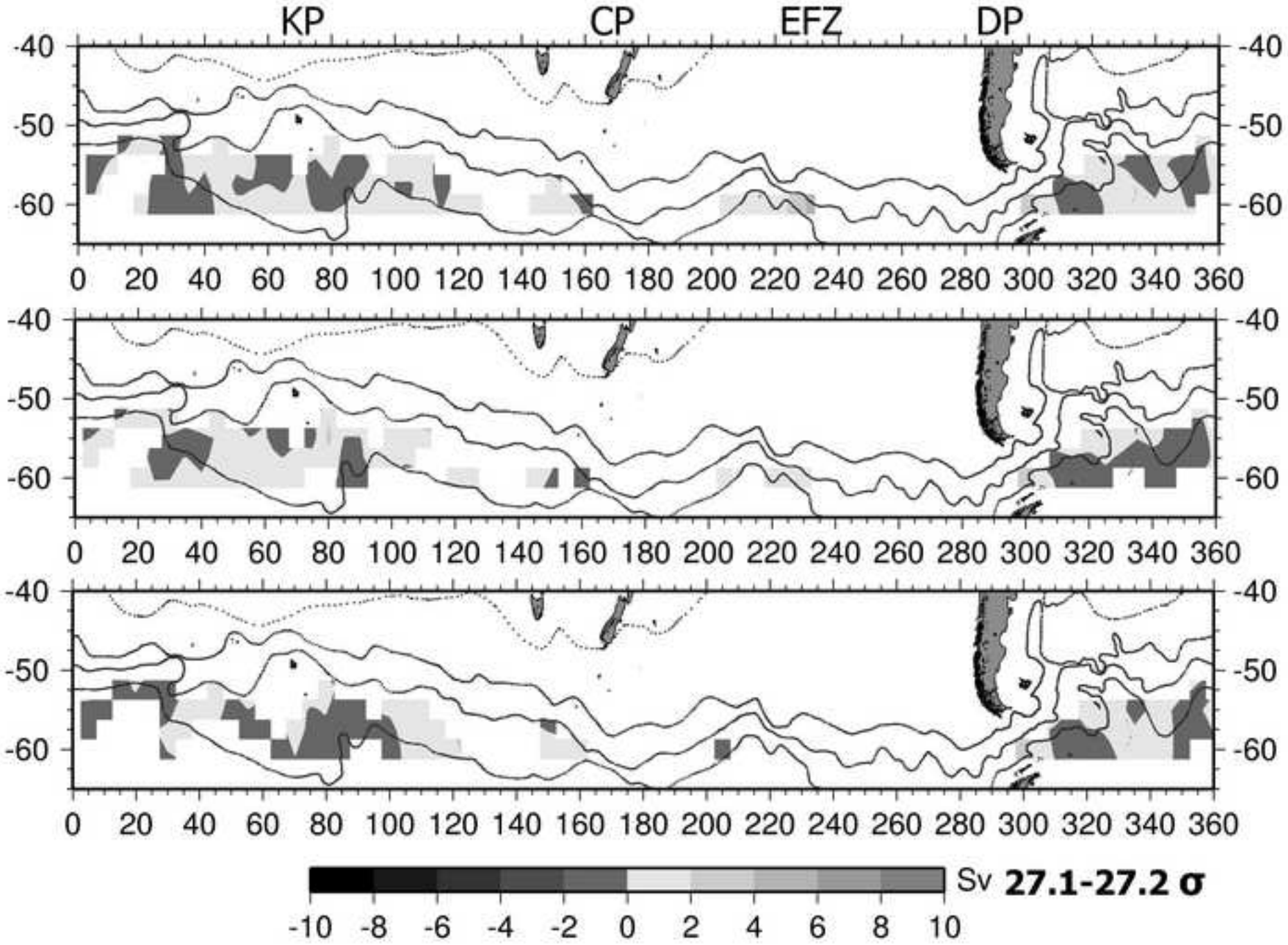

Figure 14 b&w

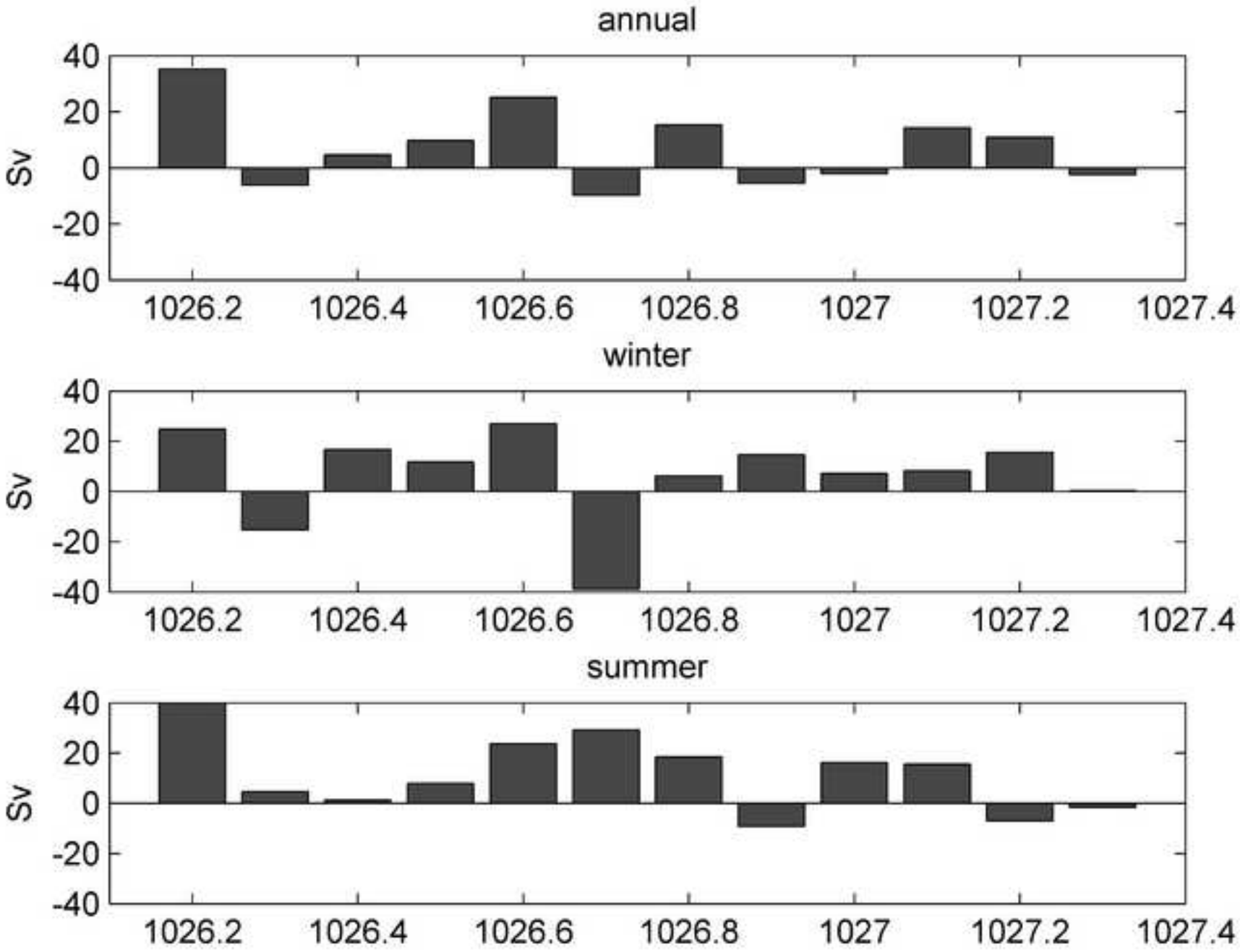

Figure 15 b&w

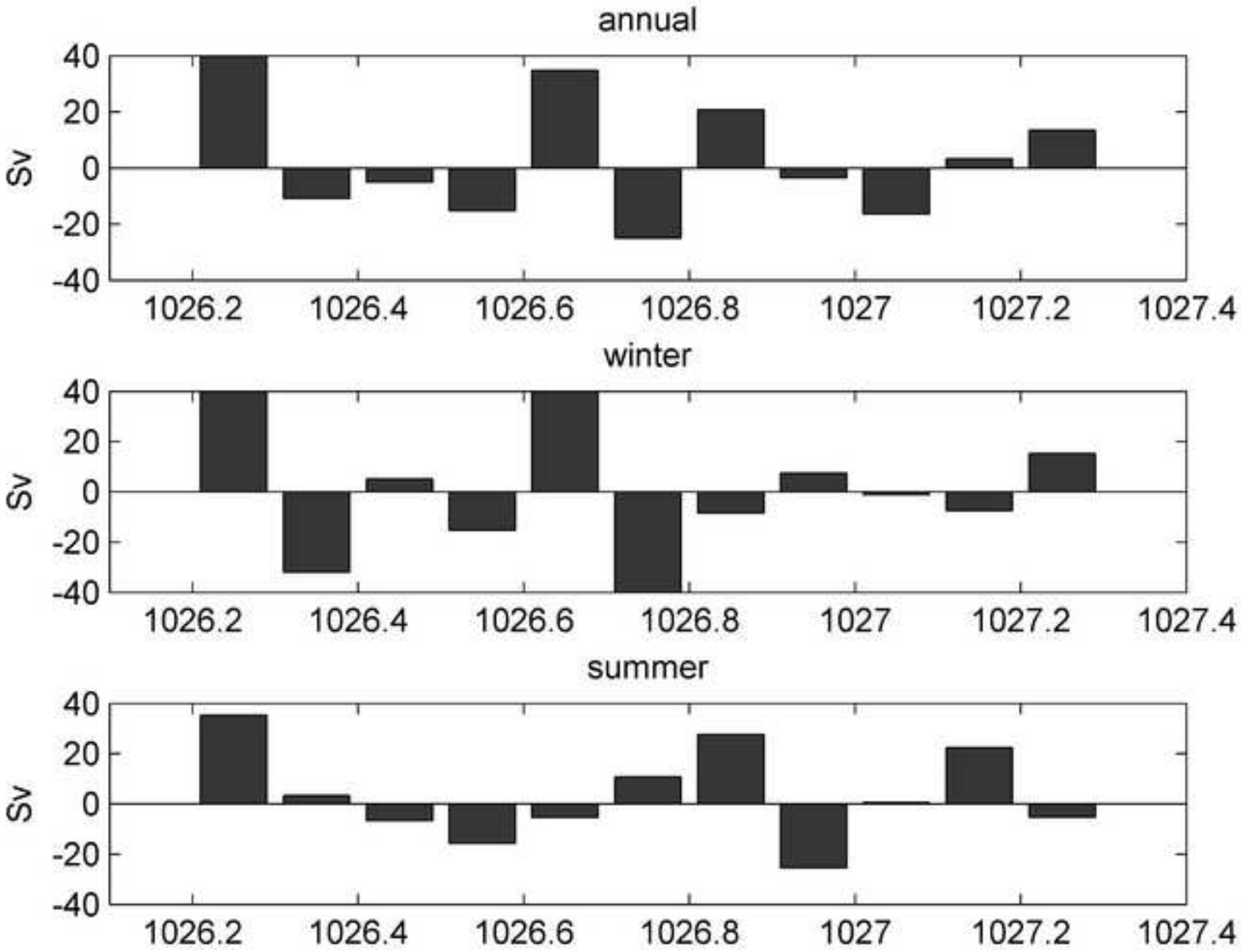

Figure 1 color

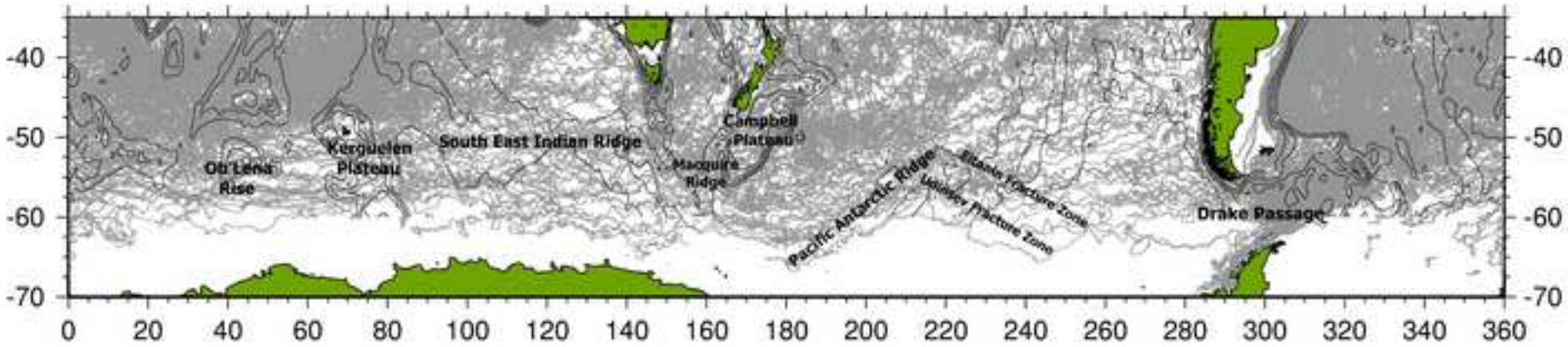

Figure 3a color

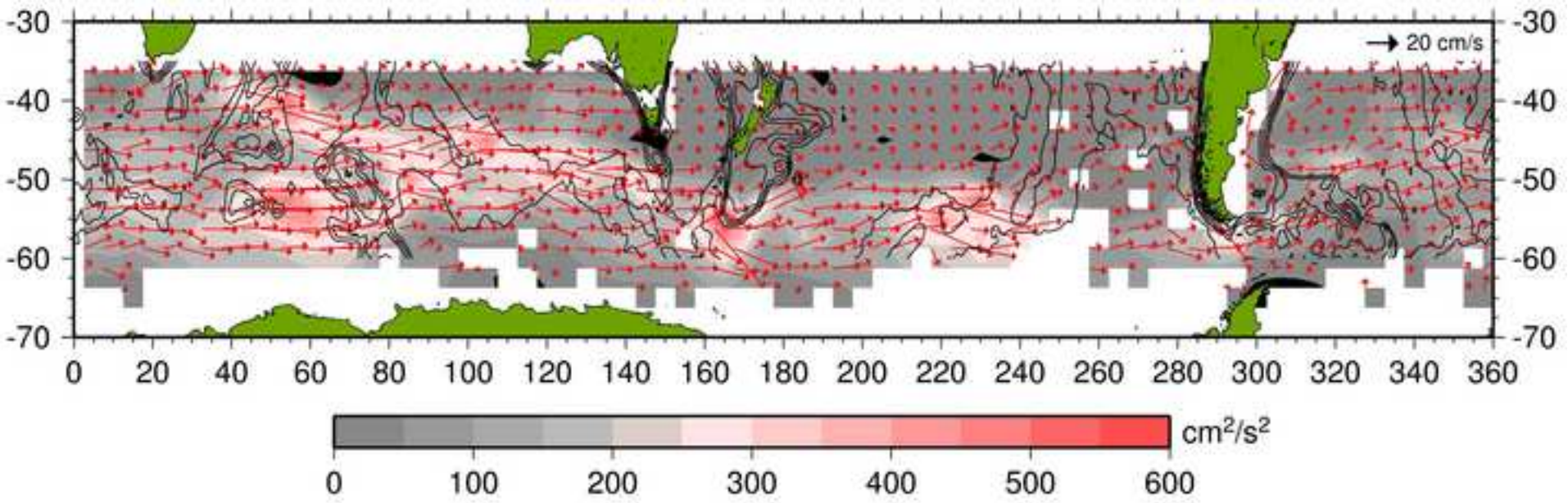

Figure 3b color

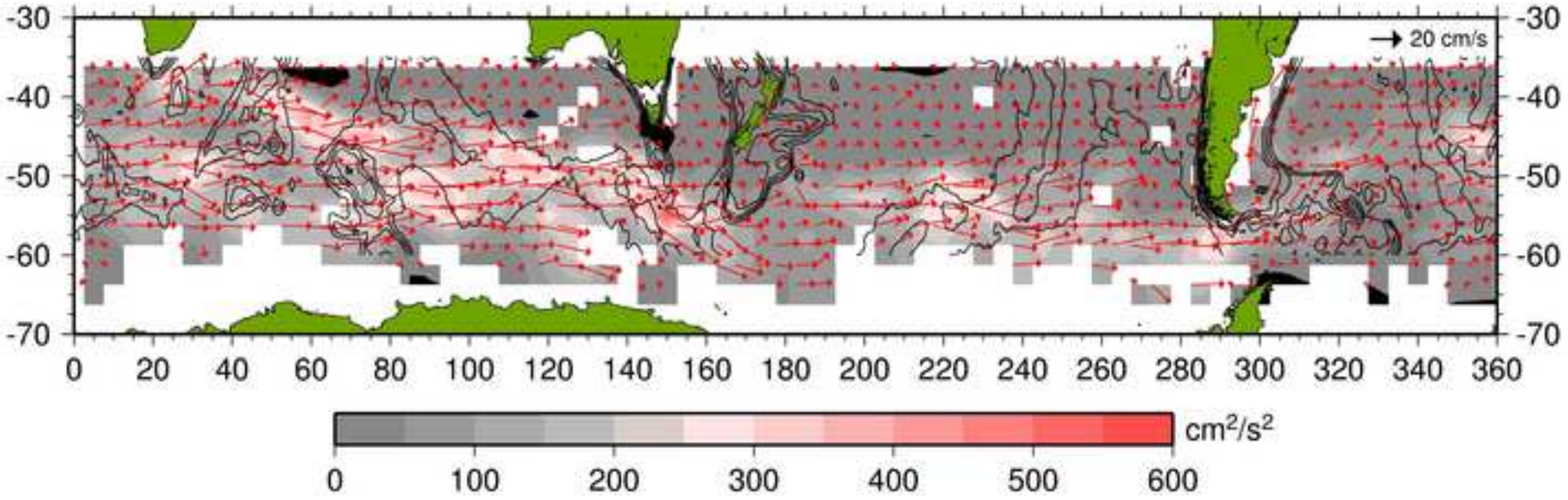

Figure 4a color

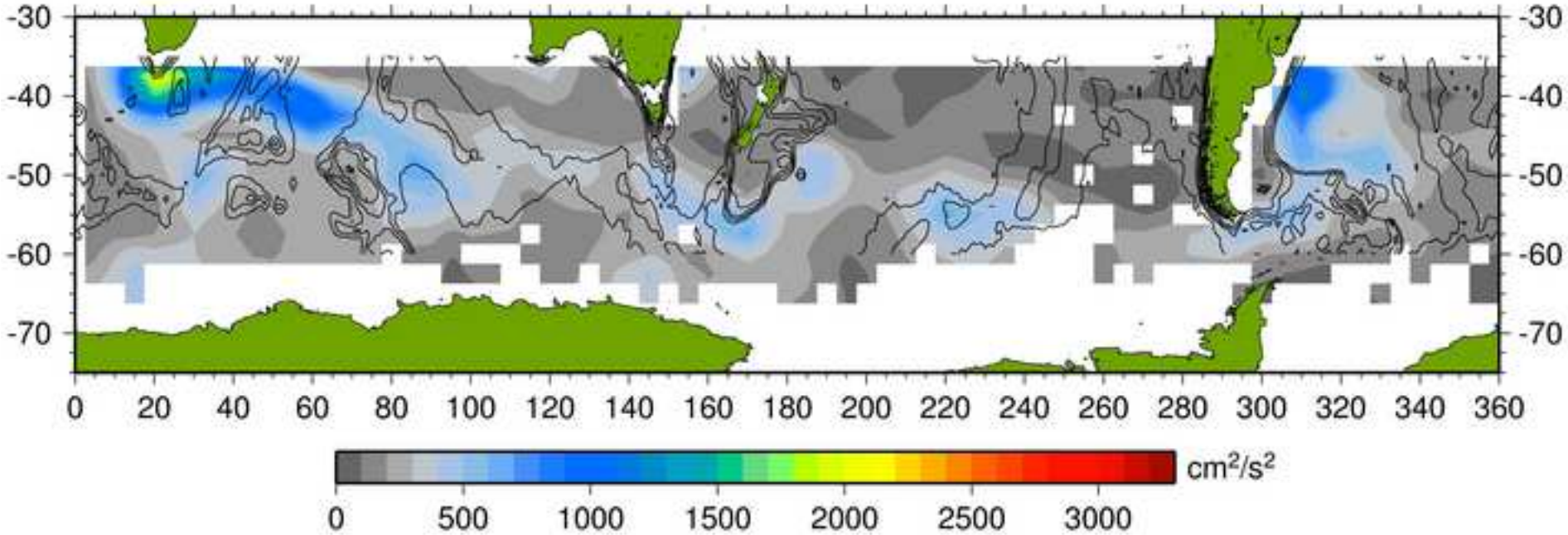

Figure 4b color

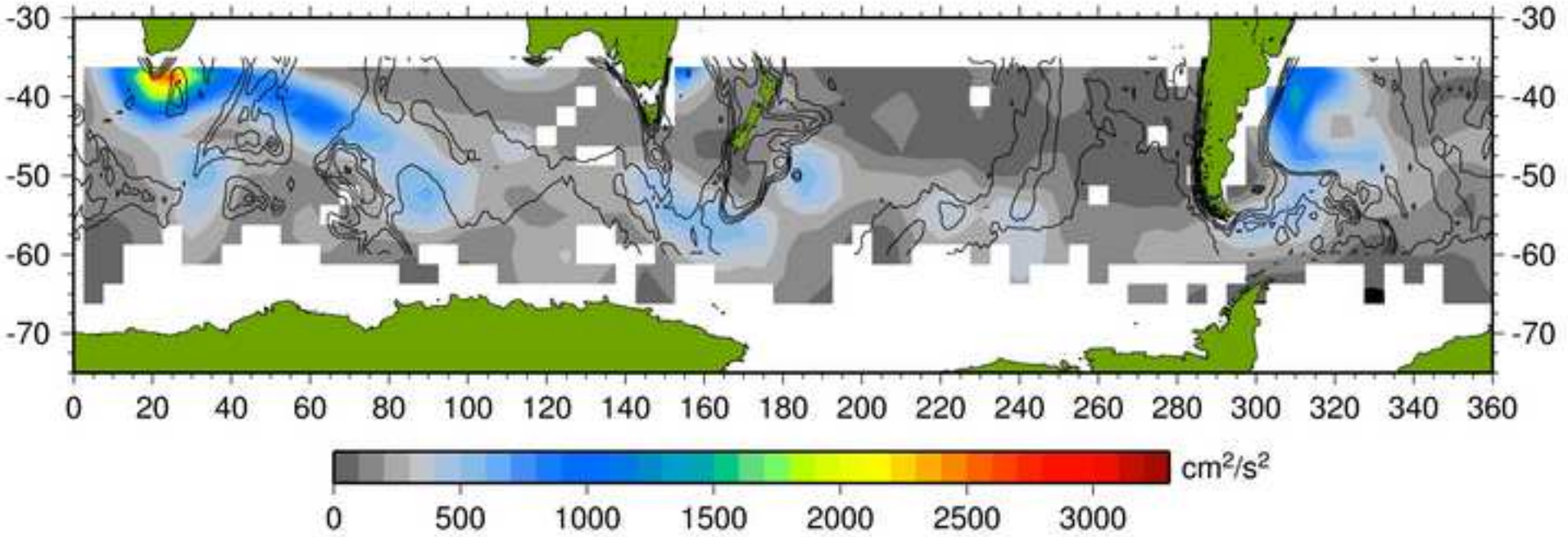

Figure 5 color

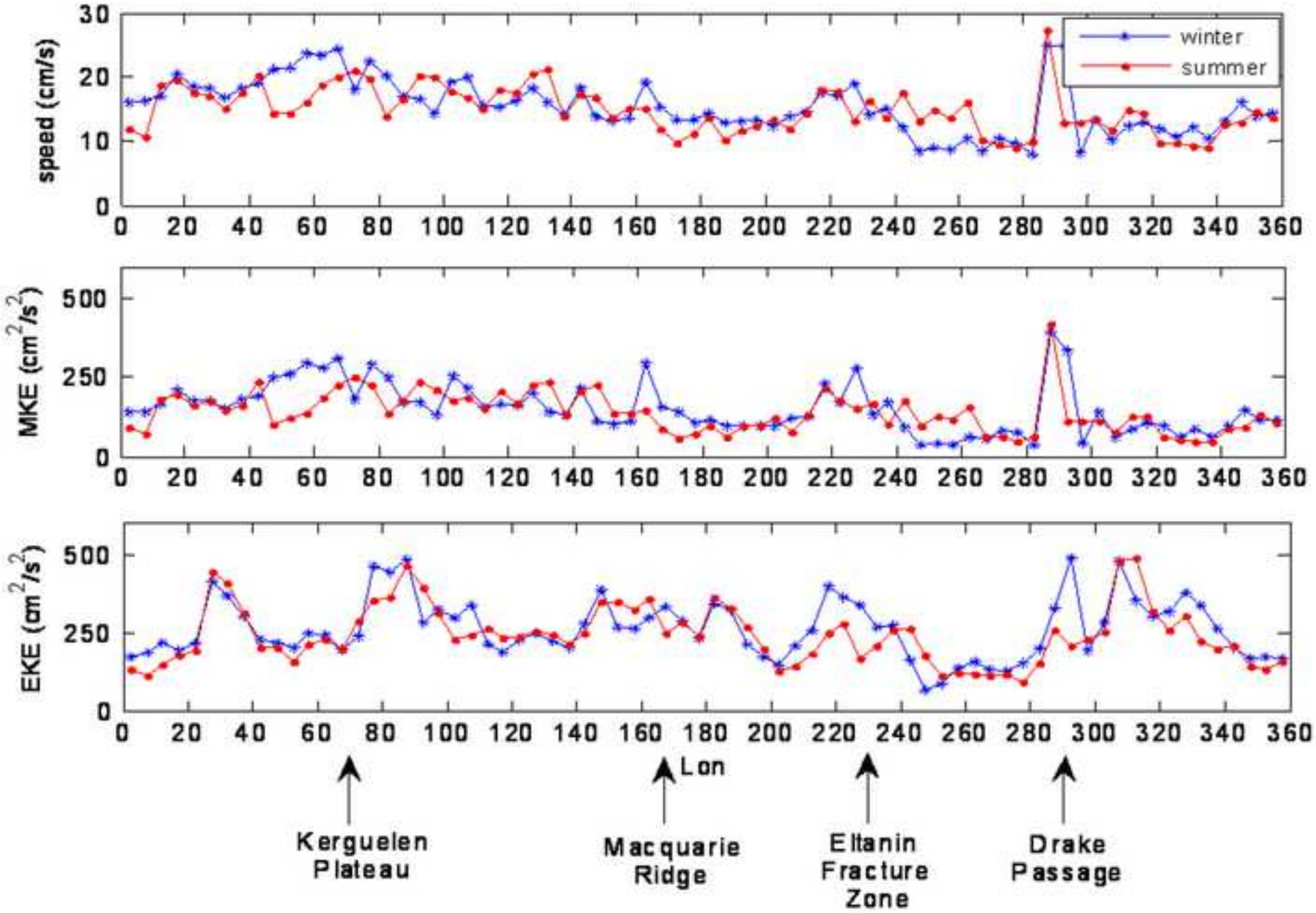

Figure 6a color

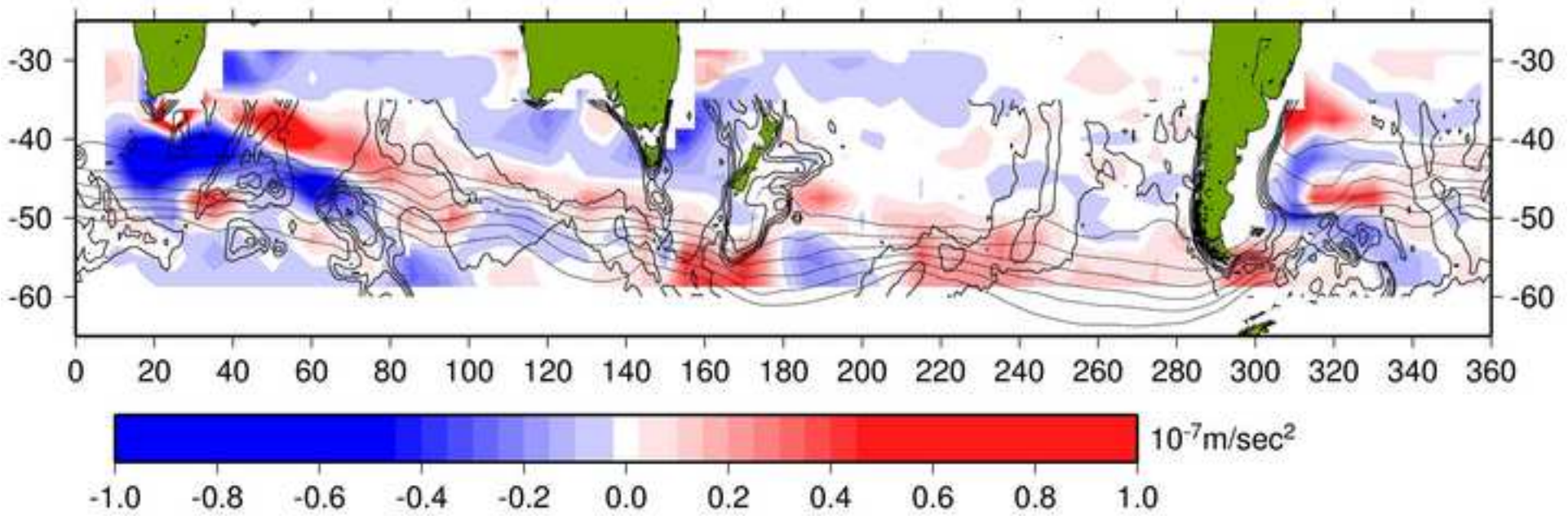

Figure 6b color

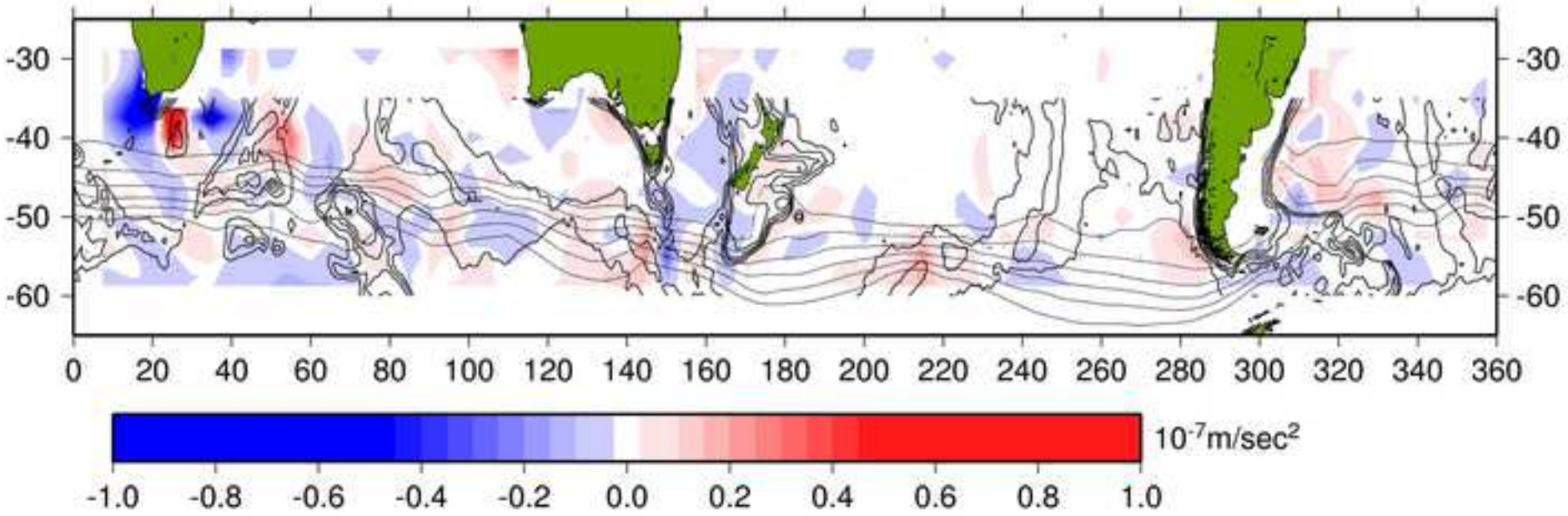

Figure 7a color

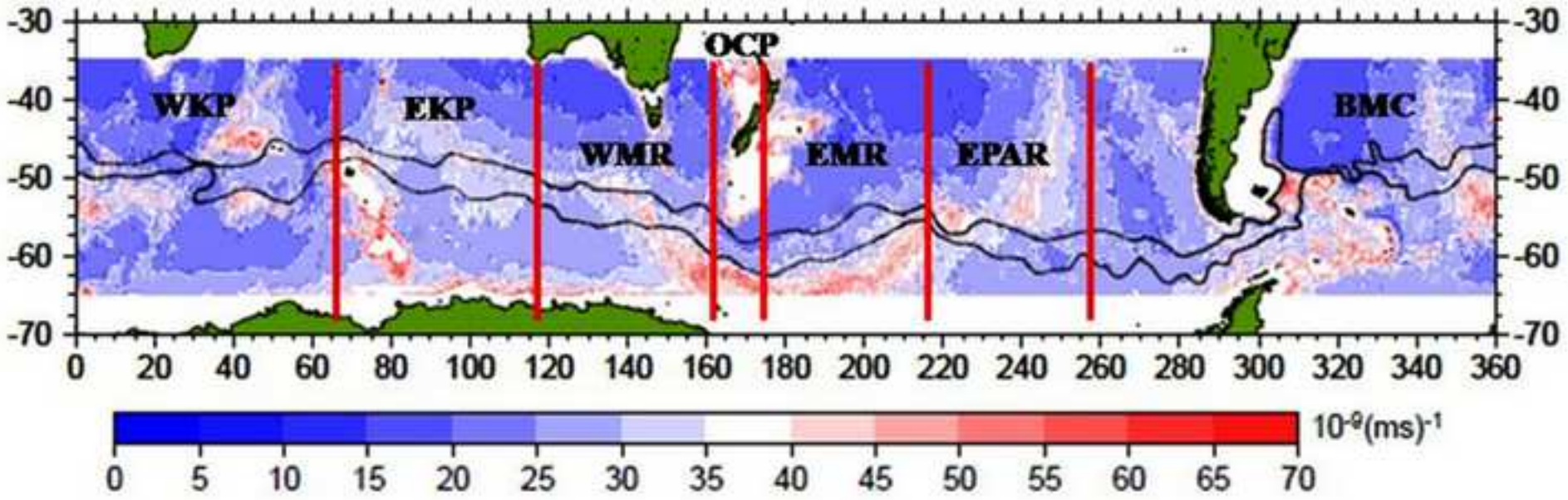

Figure 7b color

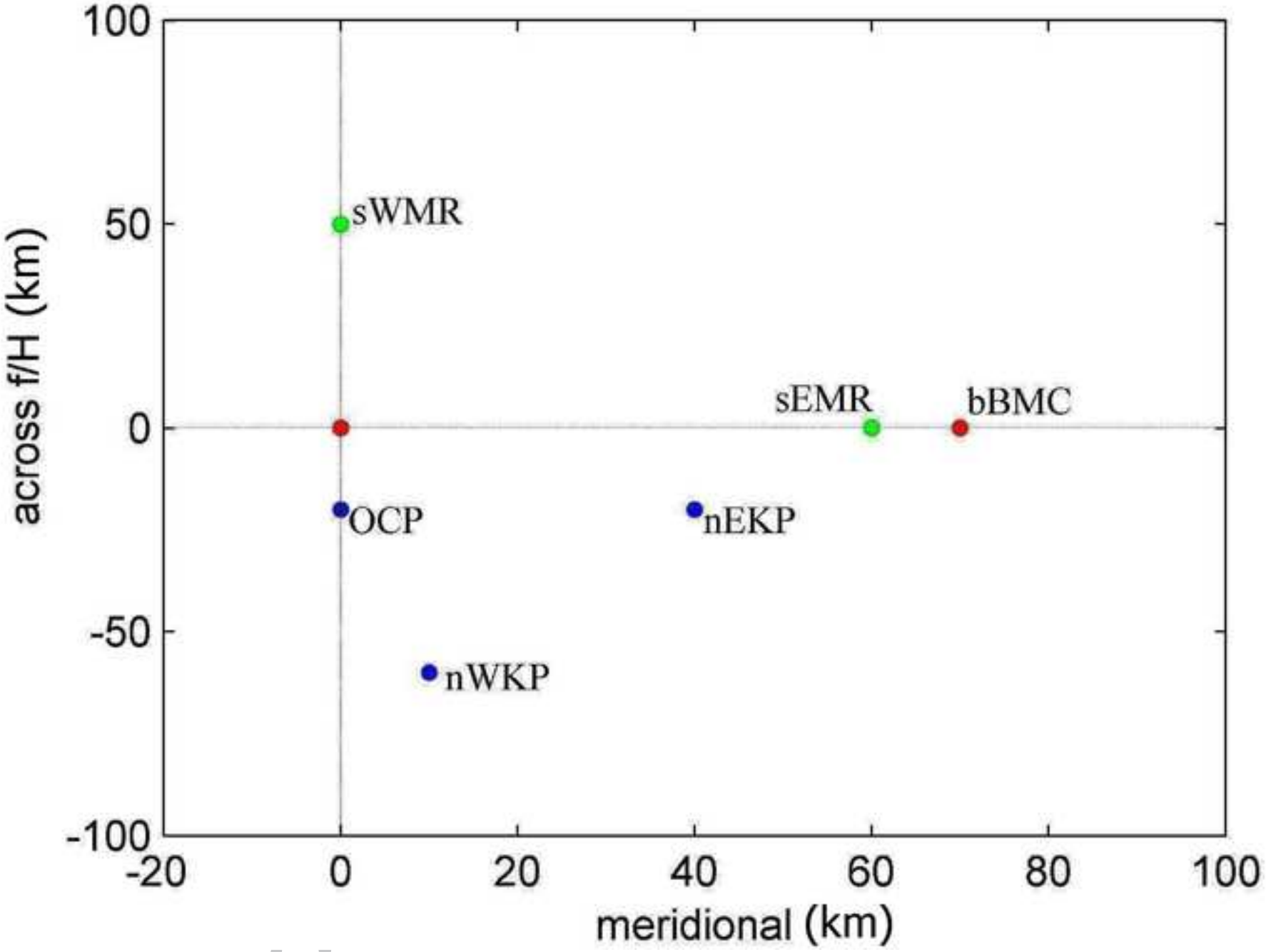

Figure 8a color

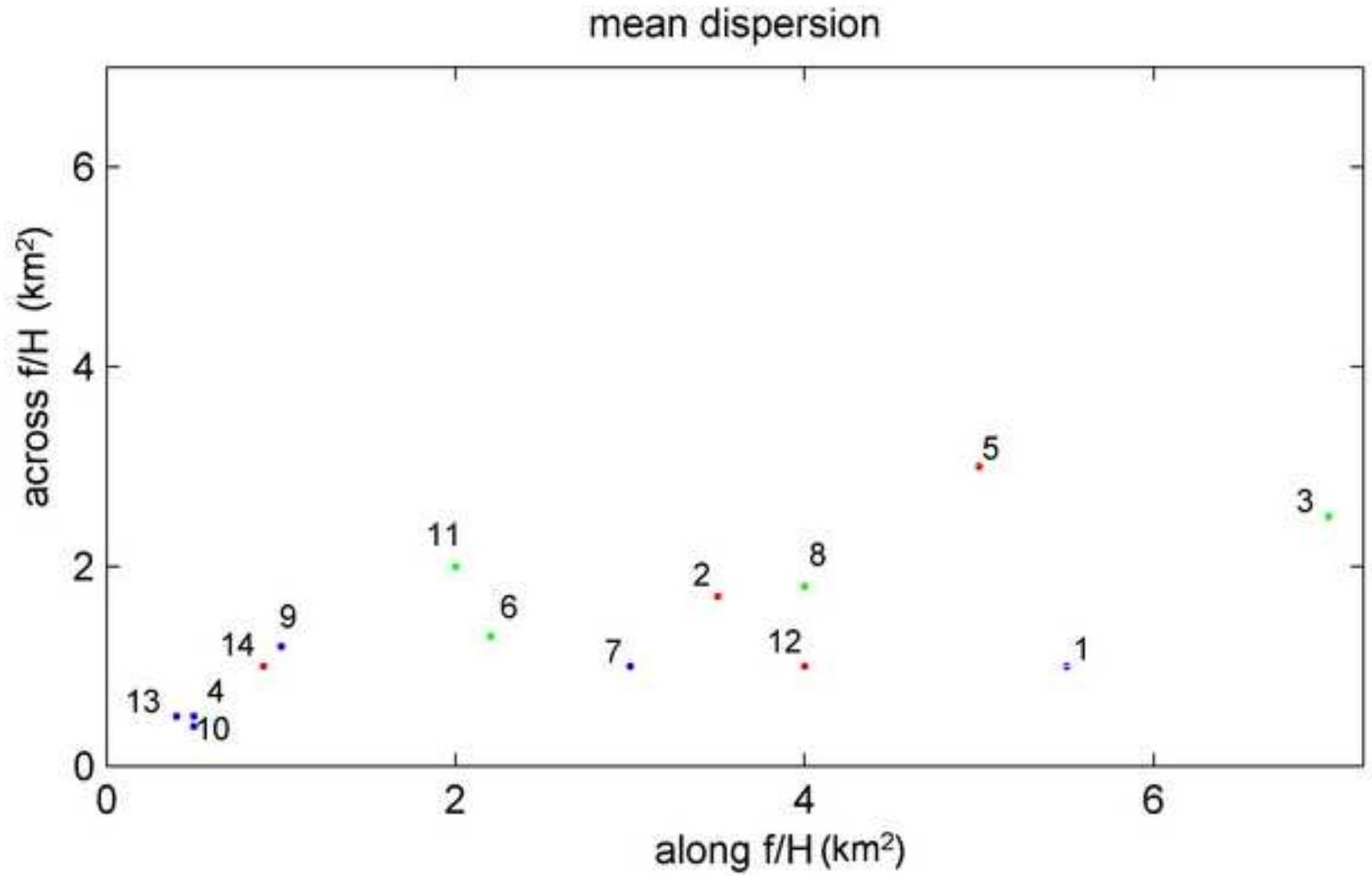

Figure 8b color

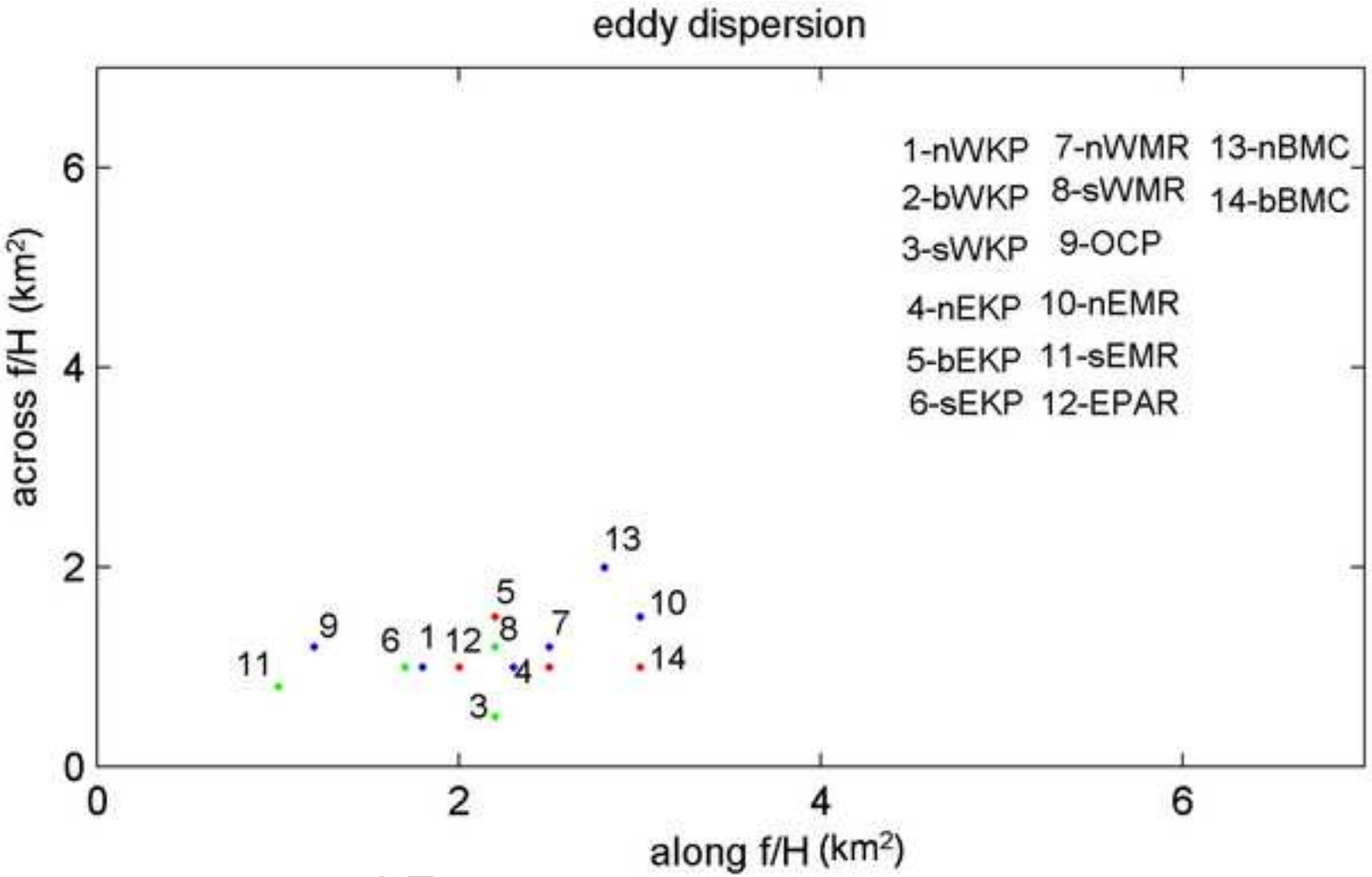

Figure 9 color

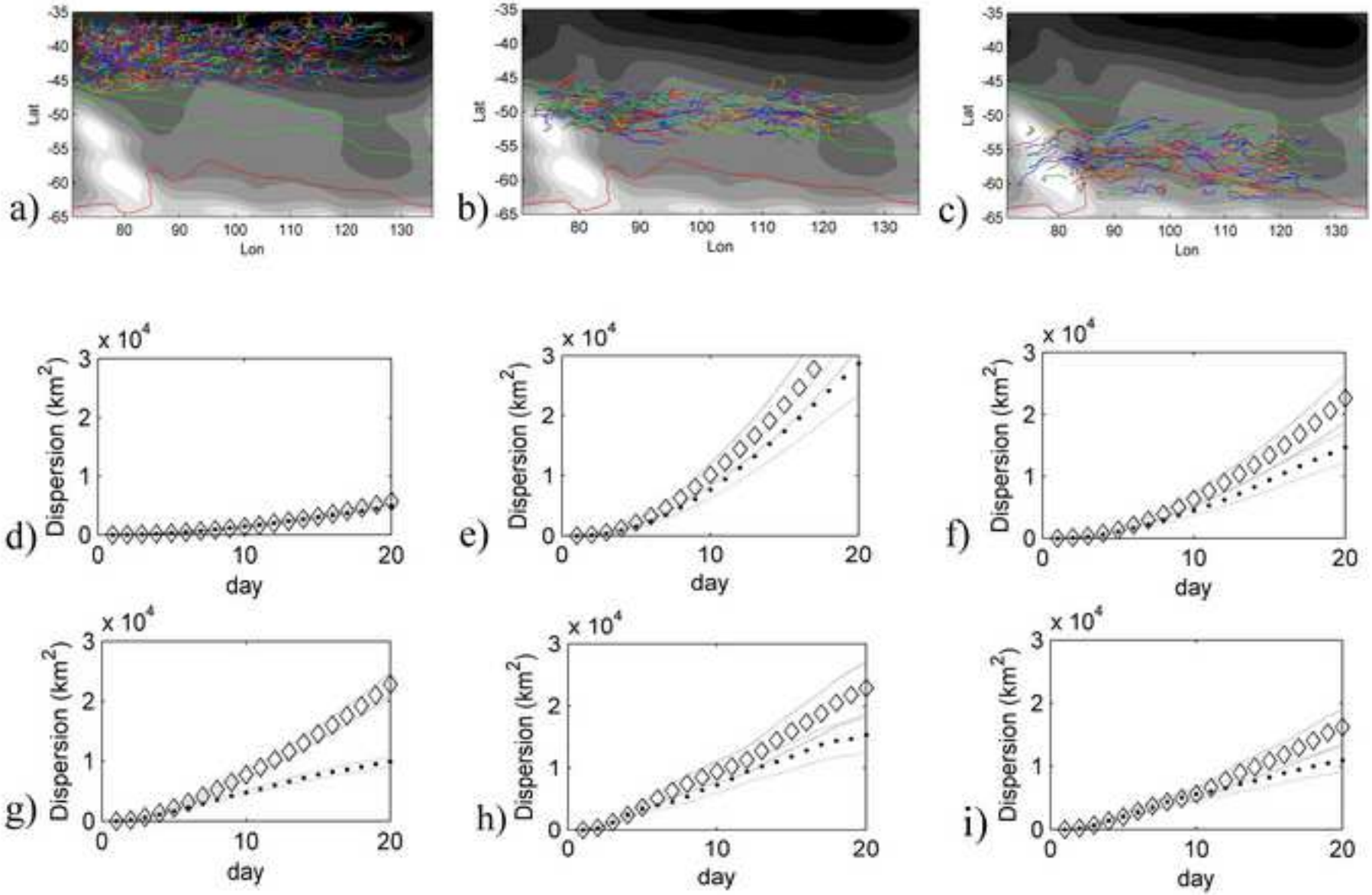

Figure 10 color

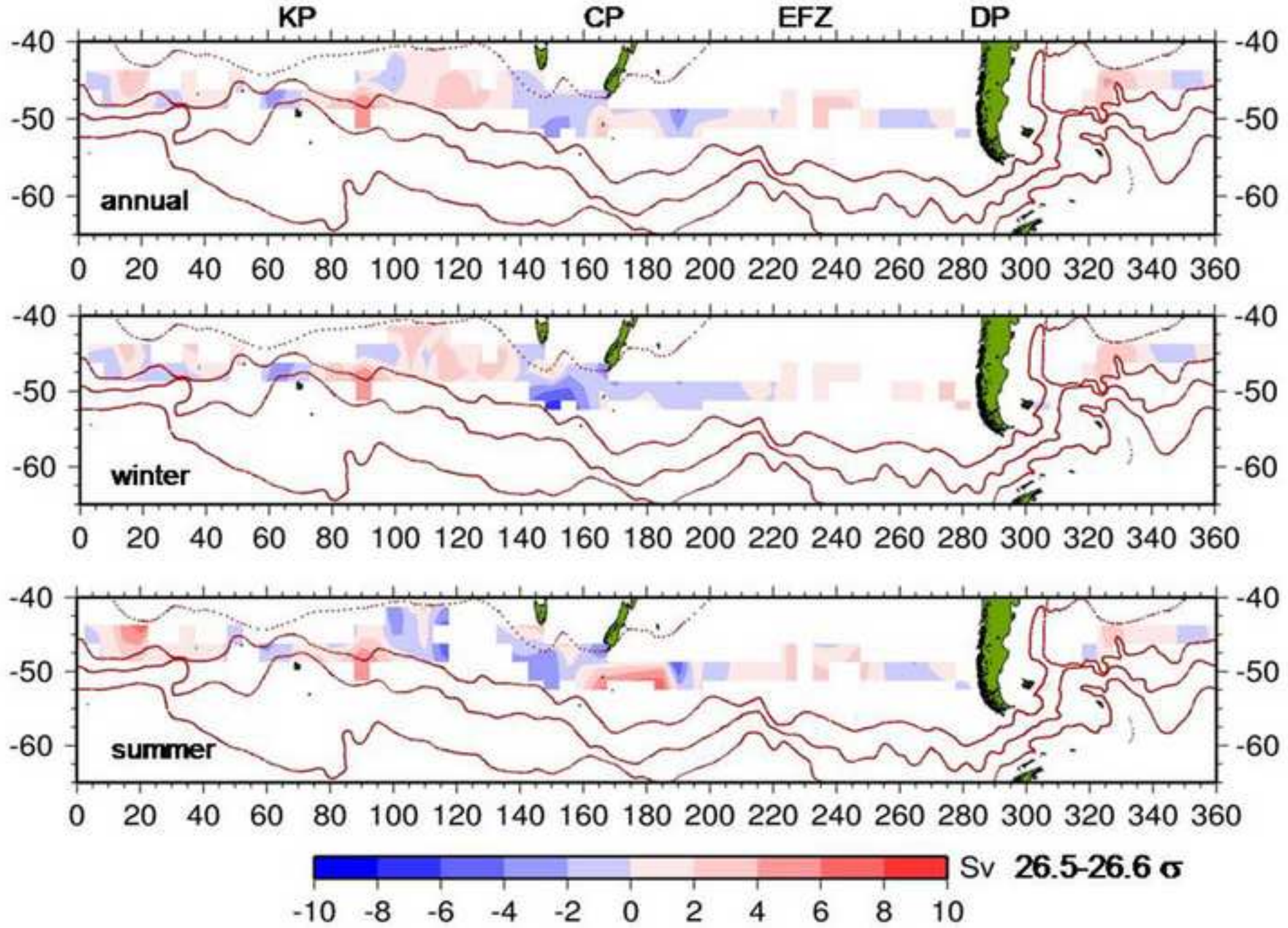

Figure 11 color

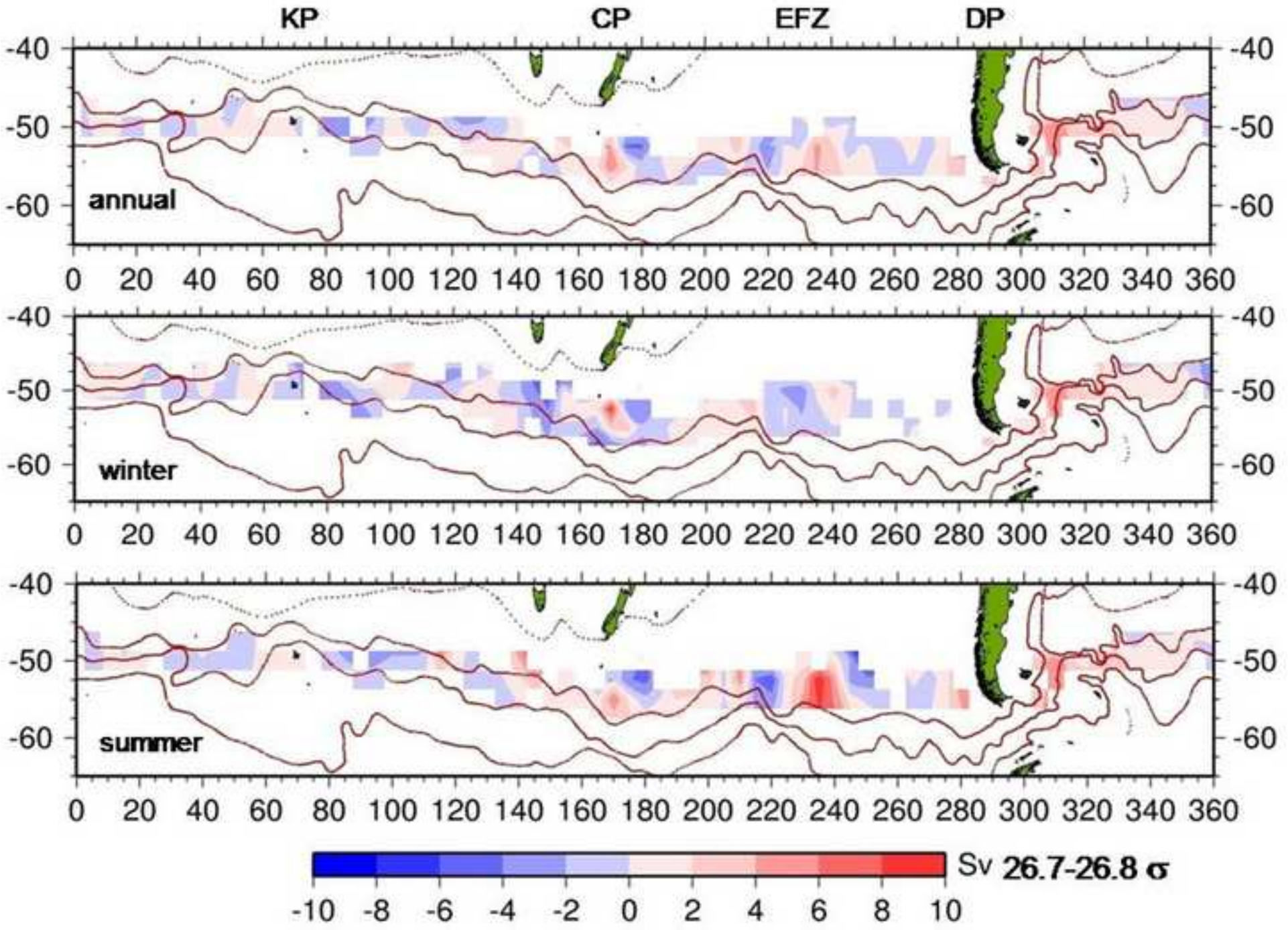

Figure 12 color

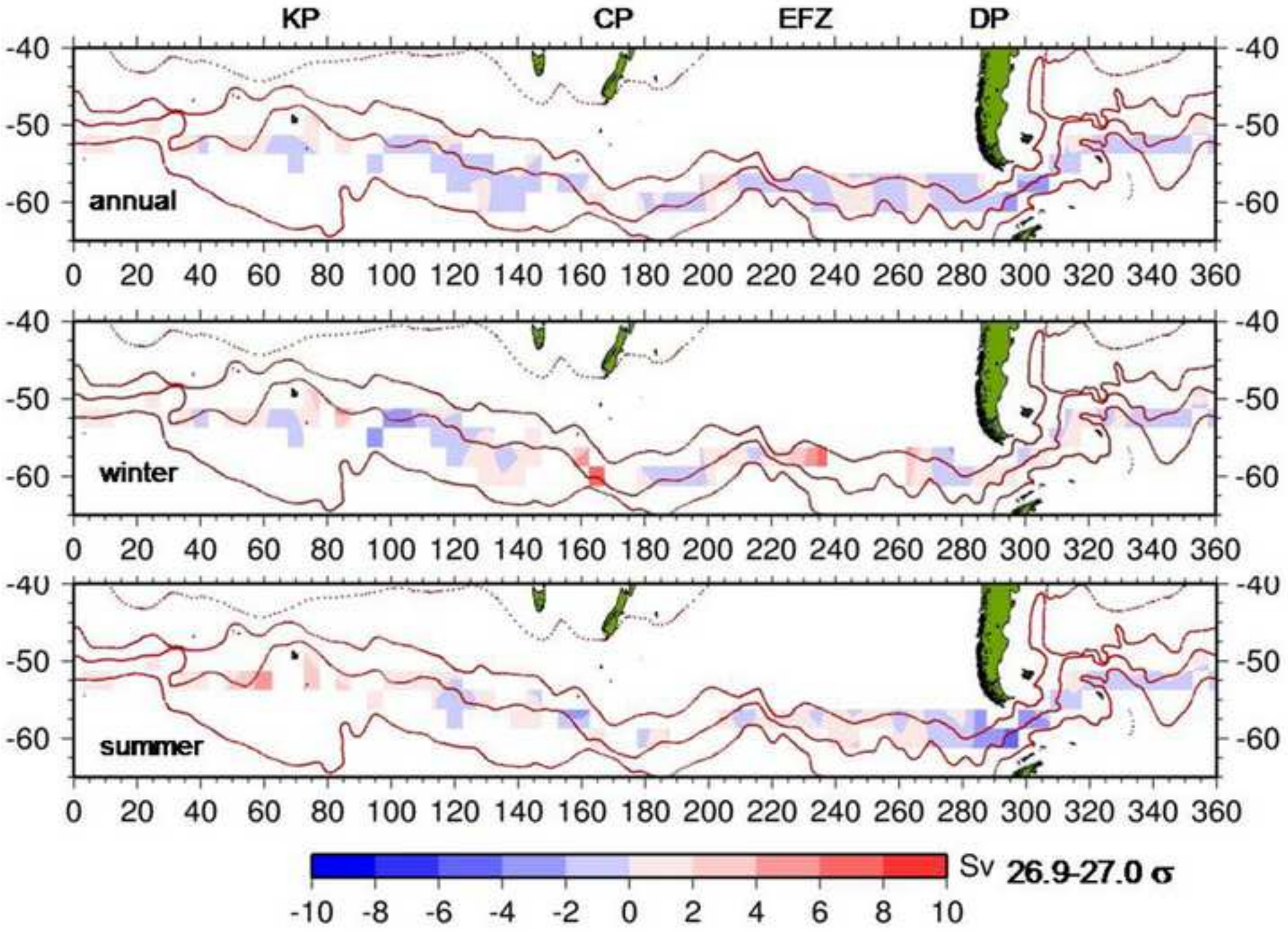

Figure 13 color

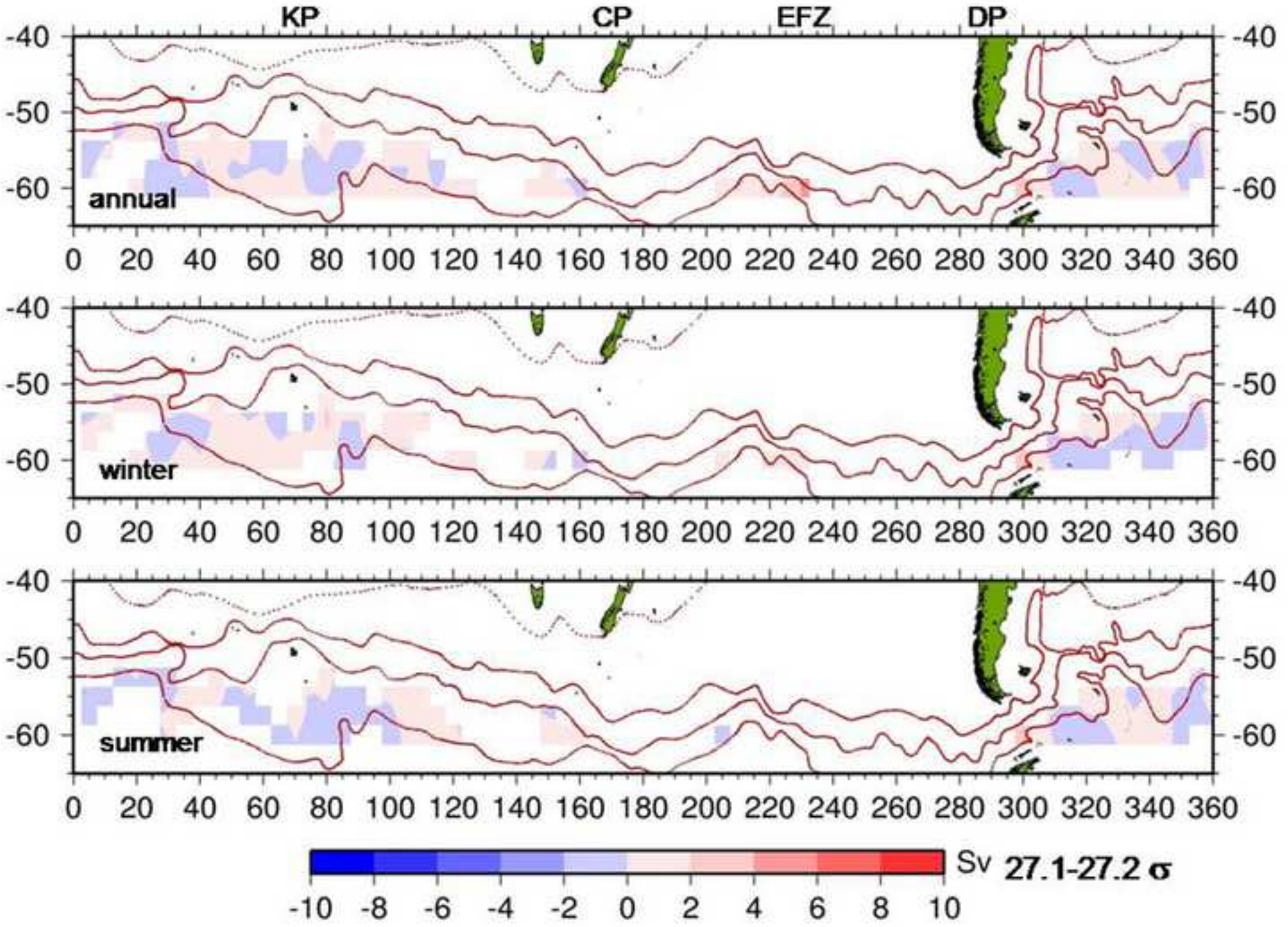

Figure 14 color

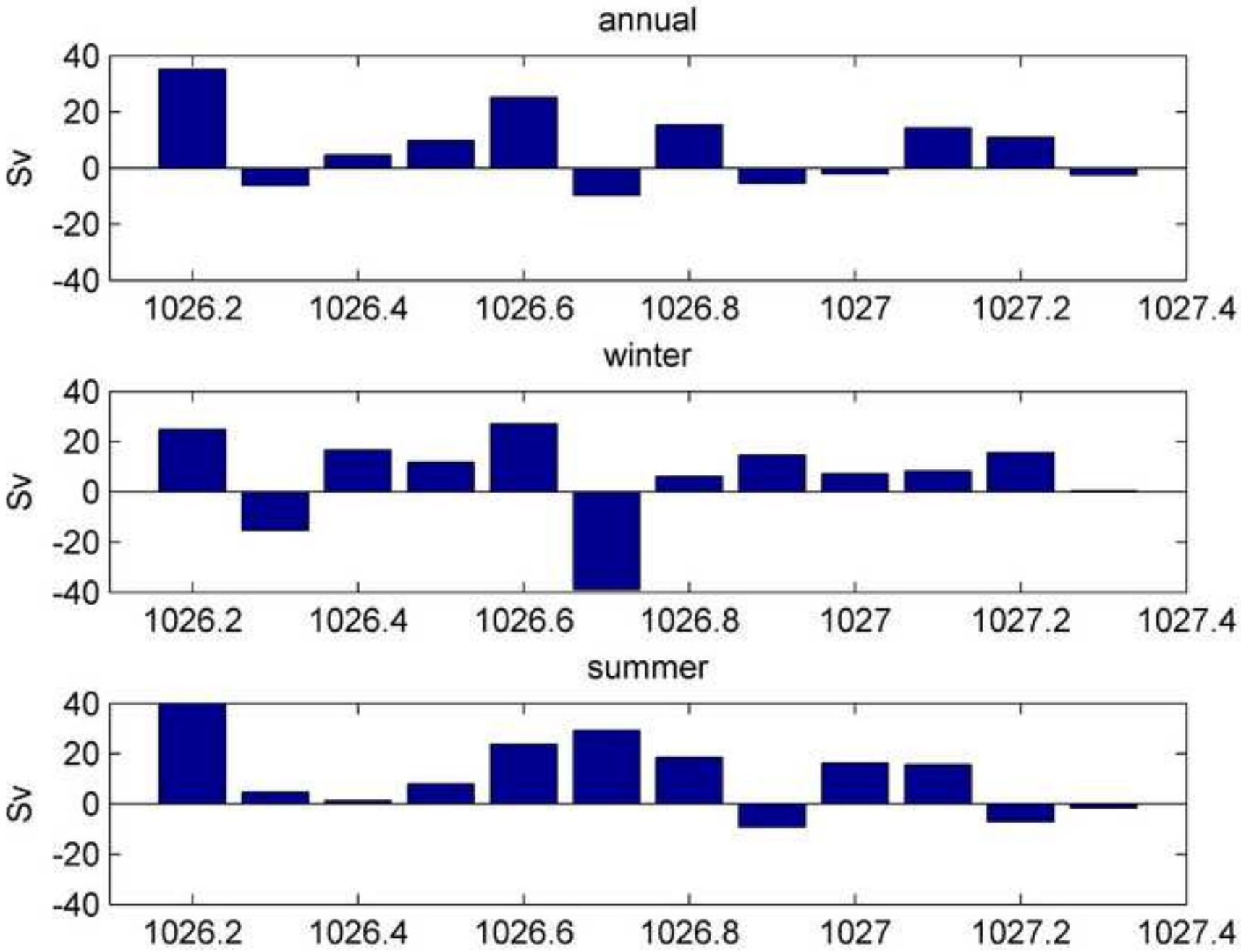

Figure 15 color

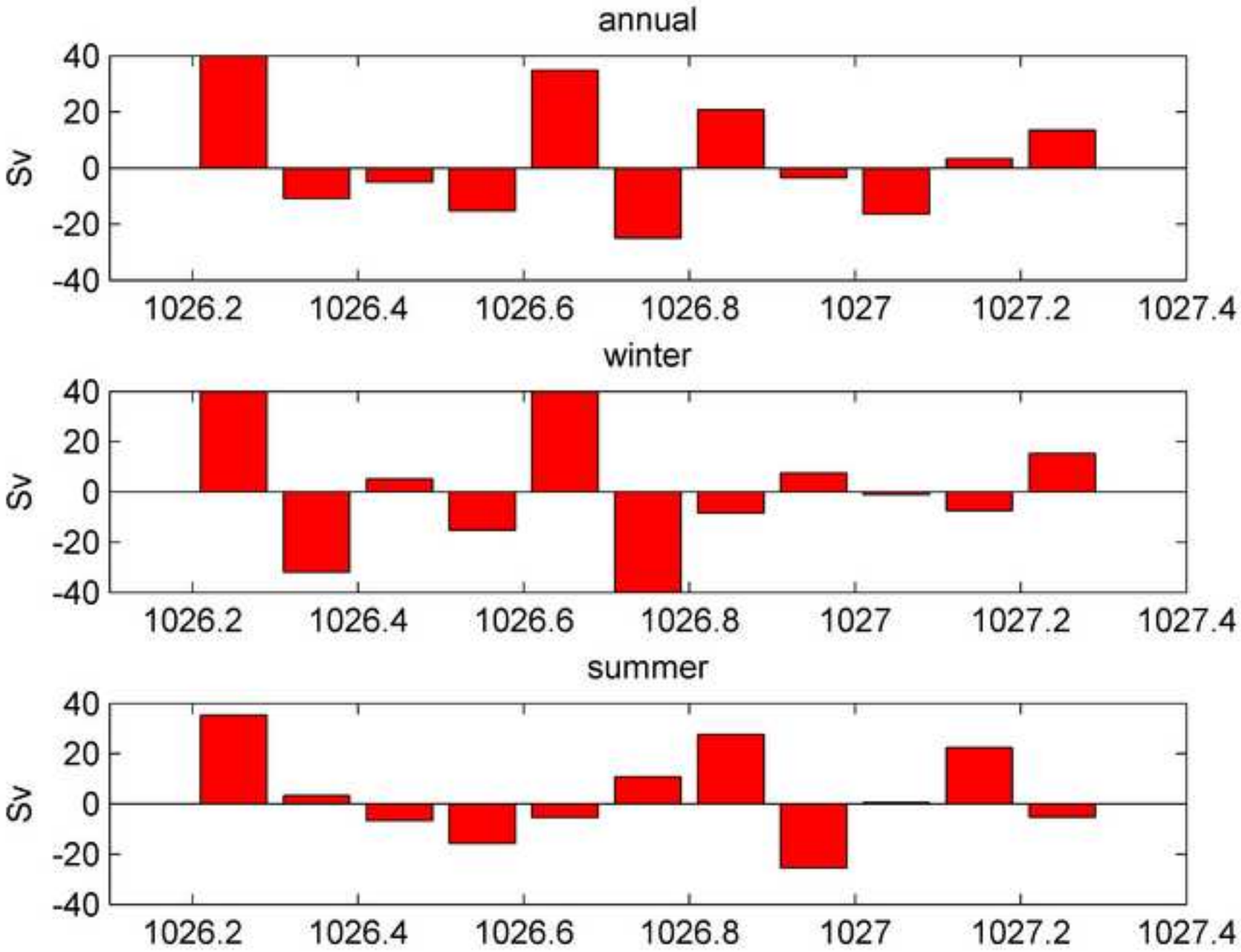

Highlights

- We use a vast dataset to study ACC eddy-mean flow and topography interactions
- Steep topography and seasonality influence locally the dispersion regime
- We examine eddy heat flow contribution to water mass subduction
- Eddy heat flow mainly contribute to enhance light SAMW formation locally